Essay on Magnetic-Wind Mills

J.L. Duarte
Dept. Electrical Engineering (Ret.)
Eindhoven University of Technology
The Netherlands

This essay explores the feasibility of autonomously operating permanent magnet motors, which can be constructed using a specific configuration of attractive and repulsive forces between magnets.

The term *magnetic-wind mill* is used to illustrate that the driving energy is sourced from a kind of continuous ”wind” that supplies energy to magnetic dipole moments, maintaining their spinning constant. This is crucial because, when mechanical energy is extracted from the mill, a counter-torque acts on the magnets, which would normally cause the intrinsic dipole moments to slow down. However, due to the fundamental principle of spin conservation, the dipole moments cannot lose energy in this way. Therefore, they must continuously receive energy from the surrounding space – the quantum vacuum – to sustain their motion.

So, the energy source originates from the ”sea of activity” within the quantum vacuum, specifically from the chaotic stochastic fluctuations of energy. Given this context, it is emphasized that the resulting excess energy deployed by the magnetic flux mills does not contradict any of the three laws of thermodynamics.

The composition of the essay is divided into three distinct sections, previously appeared as discussion papers:

Part I : Analysis and design

Considering Classical Electromagnetism (CE) (specifically the related modeling approaches for magnetic force derivation – Amperian current loops, equivalent magnetic charges, surface or volume integration of Maxwell stress tensors, scalar or vectorial formulation of virtual work principle, etc...), magnetic forces cannot do work on permanent magnets.

Nevertheless, the CE theory has significant limitations: it assumes free space is flat, and considers it a completely void structure, despite the possibility of clock measurements and distances contracting or expanding. It also relies on the premise that reference frames are always inertial, and the electromagnetic force is *a priori* postulated.

Due to these shortcomings in CE, the apparition ”magnetic-wind mill” is inevitably perceived as a ghostly occurrence. Yet, *e pur si muove*!

With this in mind, a provocative attempt is initially made in Part I, extending beyond the CE framework, by assuming that the global force aroused by one magnet acts on the ”barycenter” of the magnetic dipole moments of nearby magnets. In this scenario, it is shown that net mechanical work could indeed be achievable.

Part II : Staying power from spacetime

One of the missing links in support of the allegation that devices with only magnets seemingly generate useful energy ”out of thin air” could be *spacetime twisting*. In Part II, this concept is applied to self-rotating machines previously claimed in patents.

The mechanism of harvesting energy from the quantum vacuum by devices using permanent magnets is described based on Einstein-Cartan-Evans (ECE) theory.

The radial part of the magnetic field between rotor and stator is approximated as a circularly polarized plane wave which has a Beltrami structure, as also the vector potential has.

According to ECE, the vector potential then also describes a spacetime flux in Beltrami form. This is plausible, because, according to Tesla, such self-rotating waves are natural for the spacetime (or quantum vacuum) flux.

Mechanical torque can be created by distortions of the Beltrami flow. This can be described by a driving term in the Helmholtz equation for the vector potential.

Part III : Pathway for energy transfer

An attempt is made in Part III to describe that mechanical vibrations are not only responsible for evoking spacetime resonances, as ECE theory predicts, but could also provide a possible interface for transferring energy from the quantum vacuum to the rotating shaft of devices with only magnets. An extended Lorentz Force law based on intrinsic elementary magnetic dipole moments is applied for this purpose.

It is shown that magnetic field oscillations and mechanical vibrations interact cooperatively in a flux mill constructed with a low-rigidity structure. Notably, even quite narrow angular vibrations are sufficient to ensure the transfer of energy to the rotating parts.

Eindhoven, December 10, 2024

Access to document:
https://research.tue.nl/en/publications/essay-on-magnetic-wind-mills-parts-i-ii-iii
Supporting video:
https://www.youtube.com/watch?v=M0UFRim6r3I

Essay on Magnetic-Wind Mills
Part I : Analysis and Design

J.L. Duarte
Dept. Electrical Engineering (Ret.)
Eindhoven University of Technology
The Netherlands

***Abstract*—A methodology for the synthesis of a prime mover is presented, based only on attraction/repulsion of permanent magnets. A design example for a demonstration prototype is given, which has the potential to deploy, in theory, the sustainable generation of $22W$ mechanical power at $1000\,rpm$ and beyond.**

I. Introduction

There are quite a few methods for the description of magnetic forces as created by permanent magnets (PMs) [1]. However, although all the approaches converge to the same values in what concerns the *global* forces between PMs, the derived *local* forces are fundamentally different, implying that force density in each approach is rather a mathematical abstraction without necessarily a physical meaning [2]. Otherwise stated, consensus about a method for the *accurate* calculation of *torques* between PMs in close proximity is not found in the literature, and validation of results by experimental measurements are unavoidable [3], [4].

A commonly considered tool for modeling PMs consists on calculating magnetic forces among filamentary current loops. It is asserted in [6], on account of analytical equations starting from the Lorentz Force law, that a constrained displacement of an arrangement of filamentary current loops adds excess mechanical energy to the system moving parts, as long as the currents in the loops are kept *constant* during the closed translational orbit, and the *global* magnetic forces between loops are assumed to act concentrated on the loop geometric centers.

This modeling attempt based on centered global forces, instead of incremental *local* forces acting on loop segments, has led to similar results as vindicated in [7], where another calculation approach is used, namely the numerical solution of Maxwell stress tensors through FEM software. The outcomes in [7], [8] seemingly yield energy excess under constrained translational trajectories of PMs.

In order to pave the way for experimental verification of the provocative theoretical expectations above, this article presents the analysis and design of a first-principles-first prototype, idyllically denominated *a magnetic-wind mill*, being devised as the aggregation of simple prime-mover cells based on PMs. The magnets are modeled as the superposition of filamentary loops with constant current. However, the global magnetic forces are assumed to push the "center of mass" of the intrinsic magnetic dipole moments confined by the loops, and do not act on the Amperian currents, similar to [6]. The motivation why is considered in Section VI. In the Appendix, equivalent results are illustrated when the global forces are considered to actuate on the "center of field heaviness" of the loops.

Accordingly, the intention in the following sections is to project a device wherein the elementary cells operating together create a persistent smooth torque, sufficient to deploy enough sustainable mechanical energy for conclusive measurements. The methodology developed hereinafter details the necessary analysis tools for this purpose. The design of a small mill is presented, aiming at generating about $22W$ when rotating at $1000\,rpm$. Future experiments are planned to confirm or invalidate the feasibility of these apparently hopeless theoretical statements.

II. Elementary prime-mover cell

The concept for an initial source of motive power is shown in Fig. 1. The gearing (this case cog-wheels), assembled together with the rotors in spinning shafts, impose a constrained translation for the permanent magnets. The resulting attraction/repulsion forces among the magnets during the translational displacement lead to asymmetric torque characteristics, as shown in the sequence. A consequence of this is that, in theory, a modular structure with stacked prime-mover cells sharing the same shafts yields the sustainable generation of mechanical energy.

III. Asymmetric torque characteristics

A. Modeling of a permanent magnet

The magnetic dipole is the fundamental element of magnetism. It can be thought as a small current loop with dipole moment $\vec{m}\,[Am^2]$. Statistically, one can speak about a net magnetization $\vec{M}\,[A/m]$, representing the limit ratio of dipole moments per volume of magnetic material.

Contrary to the behavior of ferromagnetic materials, in a PM with homogeneous and uniform magnetization, there is barely interaction of the magnetic dipoles with an externally applied magnetic field. The magnetization is practically constant up to a high level of external coercive field, found to be [1]

$$\vec{M} = \frac{\vec{B}_r}{\mu_0}, \tag{1}$$

where $\vec{B}_r[T]$ is the so-called remanent magnetic flux density of the material, and $\mu_0 = 4\pi \times 10^{-7}[H/m]$ the permeability of free space.

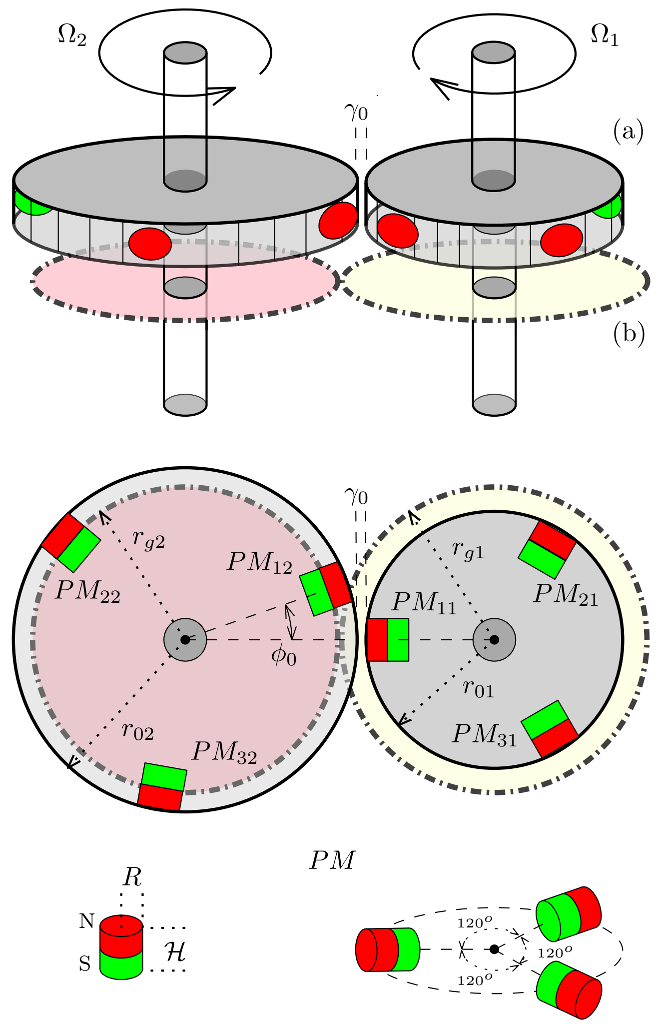

Fig. 1: Elementary prime-mover cell, consisting of (a) two rotors with embedded permanent magnets (PMs) and fixed gap separation (γ_0), and (b) a common gear mechanism, namely 1:1 cog-wheels. The angular misalignment between the rotors (ϕ_0) is kept constant by the gears in spite of rotation.

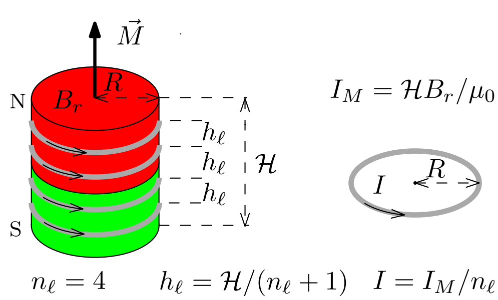

Fig. 2: Method to approximate the magnetic field created by a cylindrical PM with remanent flux density B_r as the superposition of the magnetic field engendered by n_ℓ filamentary current loops with separation h_ℓ between loops.

With regard to a PM specimen with cylindrical shape, like in Fig. 2, an analytical modeling technique is possible by assuming a fictitious magnetic surface current density on the magnet surface, given by

$$\vec{J}_M = \vec{M} \times \vec{n} \; [A/m], \tag{2}$$

where $\vec{n}$ is a unity vector normal to the cylindrical surface.

So, for a magnet with height $\mathcal{H}$, the total equivalent magnetizing current on the surface is found to become

$$I_M = \int_{\mathcal{H}} J_M \, \mathrm{d}h = \mathcal{H}B_r/\mu_0 \; [A]. \tag{3}$$

For expedient evaluation of magnetic forces through an analytical approach, the surface current in (3) is split and lumped in n_ℓ circular current loops with separation h_ℓ between loops, as shown in Fig. 2. The resulting force between magnets is then calculated as the superposition of the forces among all the equivalent current loops.

B. Current loops with constrained displacement

Two filamentary circular current loops with inner radii R_1 and R_2 and constant currents I_1 and I_2, respectively, are shown in Fig. 3, centered at points C_1 and C_2. The loop centers may translate with constant radius, r_1 and r_2, around the pivot points P_1 and P_2, such that C_1, C_2, P_1 and P_2 remain in the same plane. By given a compulsory relationship for the radial angles ϕ_1 and ϕ_2, a constrained joint trajectory for the loops is obtained. For the purpose of analysis, convenient orthogonal vector reference frames are designated in Fig. 3.

C. Reference frames

Fig. 4 illustrates the unity vectors in Fig. 3 in a frontal perspective with regard to the translation plane, showing clearly that the unity vectors $\vec{a}_{n1}$ and $\vec{a}_{n2}$ are normal to the corresponding current loop planes.

For ease of analysis, orthogonal reference frames in Figs. 3 and 4 are defined as

$$\begin{aligned}
&\vec{a}_{xj} = \vec{a}_{yj} \times \vec{a}_{zj},\ \vec{a}_{yj} = \vec{a}_{zj} \times \vec{a}_{xj}, \vec{a}_{zj} = \vec{a}_{xj} \times \vec{a}_{yj},\\
&\vec{a}_{tj} = \vec{a}_{\ell j} \times \vec{a}_{nj},\ \vec{a}_{\ell j} = \vec{a}_{nj} \times \vec{a}_{tj}, \vec{a}_{nj} = \vec{a}_{tj} \times \vec{a}_{\ell j},\\
&\text{with } \ j = \{1,2\} \ \text{ and}\\
&\vec{a}_{x2} = -\vec{a}_{x1},\ \vec{a}_{y2} = -\vec{a}_{y1},\ \vec{a}_{z2} = \vec{a}_{z1},\\
&\vec{a}_{\ell 2} = -\vec{a}_{\ell 1},\ \vec{a}_{\ell 1} = \vec{a}_{y2}\,,
\end{aligned} \tag{4}$$

where '$\times$' denotes vector cross product.

On account of the sign convention for the radial angles ϕ_1 and ϕ_2 in Fig. 4, the transformations between reference frames follow from

$$\begin{aligned}
\begin{bmatrix}\vec{a}_{tj}\\ \vec{a}_{nj}\end{bmatrix} &= \begin{bmatrix}-\sin\phi_j & \cos\phi_j\\ \cos\phi_j & \sin\phi_j\end{bmatrix}\begin{bmatrix}\vec{a}_{xj}\\ \vec{a}_{zj}\end{bmatrix},\ j=\{1,2\};\\
\begin{bmatrix}\vec{a}_{xj}\\ \vec{a}_{zj}\end{bmatrix} &= \begin{bmatrix}-\sin\phi_j & \cos\phi_j\\ \cos\phi_j & \sin\phi_j\end{bmatrix}\begin{bmatrix}\vec{a}_{tj}\\ \vec{a}_{nj}\end{bmatrix},\ j=\{1,2\};\\
\begin{bmatrix}\vec{a}_{ti}\\ \vec{a}_{ni}\end{bmatrix} &= \begin{bmatrix}\sin\phi_i & \cos\phi_i\\ -\cos\phi_i & \sin\phi_i\end{bmatrix}\begin{bmatrix}\vec{a}_{xj}\\ \vec{a}_{zj}\end{bmatrix}, i,j=\{1,2\,;\,2,1\};\\
\begin{bmatrix}\vec{a}_{xi}\\ \vec{a}_{zi}\end{bmatrix} &= \begin{bmatrix}\sin\phi_j & -\cos\phi_j\\ \cos\phi_j & \sin\phi_j\end{bmatrix}\begin{bmatrix}\vec{a}_{tj}\\ \vec{a}_{zj}\end{bmatrix},\ i,j=\{1,2\,;\,2,1\};\\
\begin{bmatrix}\vec{a}_{ti}\\ \vec{a}_{ni}\end{bmatrix} &= \begin{bmatrix}\cos\phi_{ij} & \sin\phi_{ij}\\ \sin\phi_{ij} & -\cos\phi_{ij}\end{bmatrix}\begin{bmatrix}\vec{a}_{tj}\\ \vec{a}_{nj}\end{bmatrix},\ i,j=\{1,2\,;\,2,1\};
\end{aligned} \tag{5}$$

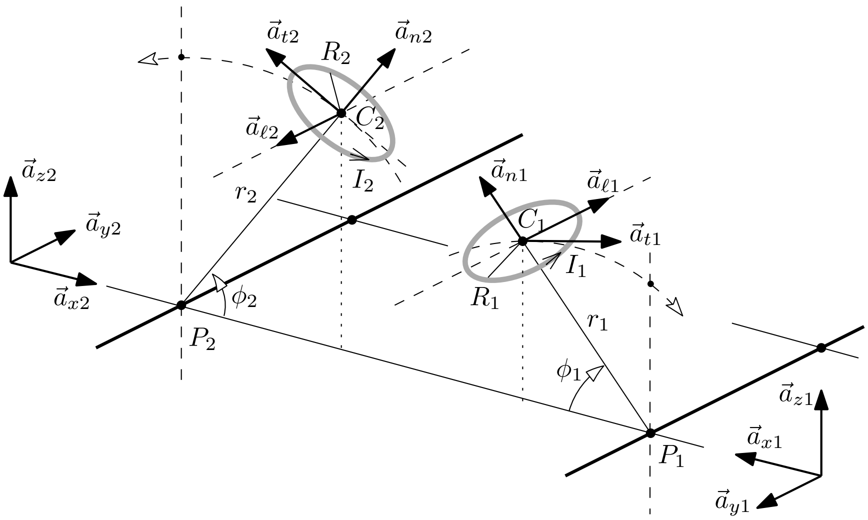

Fig. 3: Filamentary current loops with angular misalignment. The loops translate on the same plane with constant radii around fixed pivot points.

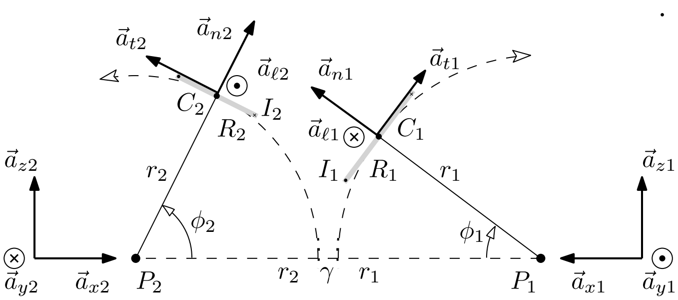

Fig. 4: Orthogonal vector reference frames from Fig. 3 shown in a frontal perspective.

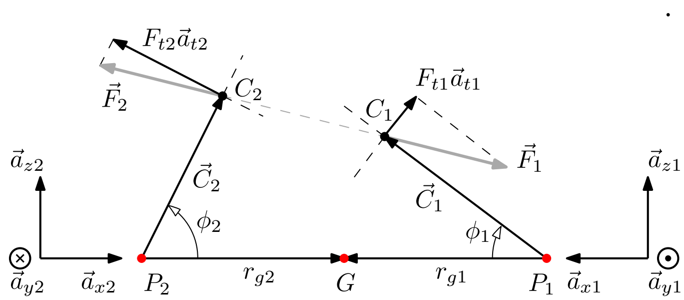

Fig. 5: Force pairs as created by magnetic repulsion/attraction between current loops constrained by cog-wheels. The forces are assumed to act on the loop geometric centers.

with

$$\phi_{12} = \phi_{21} = \phi_1 + \phi_2 \,. \tag{6}$$

It is also assumed in Fig. 4 that the sum $r_1 + \gamma + r_2$ is constant, being equal to

$$r_1 + \gamma + r_2 = \Sigma_0 = r_{02} + \gamma_0 + r_{01}, \tag{7}$$

where $r_1 \leq r_{01},\ r_2 \leq r_{02},\ \gamma \geq \gamma_0$, with r_{01}, r_{02}, γ_0 defined in Fig. 1.

As an example of frame transformation, the vector linking the loop centers C_1 to C_2,

$$\begin{aligned}
\vec{C}_{21} &= r_2\vec{a}_{n2} + \Sigma_0\vec{a}_{x1} - r_1\vec{a}_{n1}\ , \\
\vec{C}_{21} &= \begin{bmatrix} r_2\cos\phi_2 & r_2\sin\phi_2 \end{bmatrix} \begin{bmatrix} \vec{a}_{x2} \\ \vec{a}_{z2} \end{bmatrix} + \begin{bmatrix} \Sigma_0 & 0 \end{bmatrix} \begin{bmatrix} \vec{a}_{x1} \\ \vec{a}_{z1} \end{bmatrix} + \\
&+ \begin{bmatrix} r_1\cos\phi_1 & r_1\sin\phi_1 \end{bmatrix} \begin{bmatrix} \vec{a}_{x1} \\ \vec{a}_{z1} \end{bmatrix},
\end{aligned}$$

when referenced to $(\vec{a}_{t1}, \vec{a}_{n1})$, can be found from (5) as

$$\begin{aligned}
\vec{C}_{21} &= -\left(\Sigma_0 \sin\phi_1 - r_2\sin\phi_{12}\right)\vec{a}_{t1} \\
&\quad + \left(\Sigma_0\cos\phi_1 - r_2\cos\phi_{12} - r_1\right)\vec{a}_{n1}.
\end{aligned} \tag{8}$$

D. *Static forces and torques*

Fig. 5 illustrates a static situation, showing the magnetic forces on the current loops in Fig. 3 when a gearing such as cog-wheels is applied. The loop centers are located at

$$\vec{C}_1 = r_1\,\vec{a}_{n1} \ \text{ and } \ \vec{C}_2 = r_2\,\vec{a}_{n2} \tag{9}$$

relatively to the pivot points P_1 and P_2, respectively. Point G is fixed in space and lies at the interface contact between sides of the cog-wheels in Fig. 1, the gearing having also pivot points at P_1 and P_2 and constant radii r_{g1} and r_{g2}, with gear ratio $\rho_{21} = r_{g2}/r_{g1} = 1$. Also note, with regard to Fig.4 and (7), that $r_{g1} + r_{g2} = \Sigma_0$.

The resulting magnetic forces actuating on the current loops, $\vec{F}_1$ and $\vec{F}_2$, form a repulsion/attraction pair, that is,

$$\vec{F}_1 + \vec{F}_2 = 0. \tag{10}$$

These *global* forces originate from the integration of magnetic forces on incremental current loop segments, and can be determined following the approach in [**?**] (also detailed in [6]). For ease of derivation, it is convenient to consider the total force $\vec{F}_2$ on loop #2, which is a consequence of current circulation through loop #1, with reference to a vectorial frame placed on loop #1 as

$$\vec{F}_2 = \mathcal{F}_{t21}\,\vec{a}_{t1} + \mathcal{F}_{n21}\,\vec{a}_{n1}, \tag{11}$$

since $\mathcal{F}_{t21} \equiv \mathcal{F}_{t21}(\phi_1, \phi_2), \mathcal{F}_{n21} \equiv \mathcal{F}_{n21}(\phi_1, \phi_2)$ may be then determined by purely analytical equations. Eventually, when necessary to consider $\vec{F}_2$ with reference to a frame placed on loop #2 as

$$\vec{F}_2 = F_{t2}\,\vec{a}_{t2} + F_{n2}\,\vec{a}_{n2}, \tag{12}$$

it results from (4) and (11) that

$$\begin{aligned} \vec{F}_2 &= \begin{bmatrix} \mathcal{F}_{t21} & \mathcal{F}_{n21} \end{bmatrix} \begin{bmatrix} \vec{a}_{t1} \\ \vec{a}_{n1} \end{bmatrix}, \\ \vec{F}_2 &= \begin{bmatrix} \mathcal{F}_{t21} & \mathcal{F}_{n21} \end{bmatrix} \begin{bmatrix} \cos\phi_{12} & \sin\phi_{12} \\ \sin\phi_{12} & -\cos\phi_{12} \end{bmatrix} \begin{bmatrix} \vec{a}_{t2} \\ \vec{a}_{n2} \end{bmatrix}, \end{aligned}$$

leading to

$$F_{t2} = \mathcal{F}_{t21}\cos\phi_{12} + \mathcal{F}_{n21}\sin\phi_{12}, \tag{13}$$

$$F_{n2} = \mathcal{F}_{t21}\sin\phi_{12} - \mathcal{F}_{n21}\cos\phi_{12}\,. \tag{14}$$

Similarly, the total force $\vec{F}_1$ exerted on loop #1 due to current circulation through loop #2 is referenced to a frame placed on loop #1 as

$$\vec{F}_1 = F_{t1}\,\vec{a}_{t1} + F_{n1}\,\vec{a}_{n1}\,. \tag{15}$$

Thereby, from (10), (11) and (15) follows

$$F_{t1} = -\mathcal{F}_{t21} \;\;\&\;\; F_{n1} = -\mathcal{F}_{n21}\,. \tag{16}$$

Once $\mathcal{F}_{t21}(\phi_1, \phi_2), \mathcal{F}_{n21}(\phi_1, \phi_2)$ are known, under the supposition that the magnetic forces are concentrated on the geometric loop centers (more about that in Section VI), the associated torques in Fig. 5 can be readily described. For instance, the resulting torque $\vec{T}_2$ around the pivot point P_2 is given by

$$\vec{T}_2 = \vec{C}_2 \times \vec{F}_2 - \rho_{21}\left(\vec{C}_1 \times \vec{F}_1\right), \quad \text{or} \tag{17}$$

$$\vec{T}_2 = -T_2(\phi_1, \phi_2)\,\vec{a}_{y2}, \tag{18}$$

where $\rho_{21} = r_{g2}/r_{g1}$ is the gear ratio. The minus sign in (18) has been introduced for later display convenience, indicating that $\vec{T}_2$ acts in the c.c.w. direction when $T_2(\phi_1, \phi_2) > 0$. Combining (9), (11), (15) and (17), after some manipulations it is found that in (18)

$$T_2(\phi_1, \phi_2) = (r_2\cos\phi_{12} - \rho_{21}r_1)\mathcal{F}_{t21} + (r_2\sin\phi_{12})\mathcal{F}_{n21} \tag{19}$$

When ϕ_1 and ϕ_2 are constrained as

$$\phi_1 = \rho_{21}\theta \;\;\&\;\; \phi_2 = \theta + \phi_0 \;\; \text{with}\; \theta = \int \mathrm{d}\theta\,, \tag{20}$$

it is shown in the following section that, for a special choice of parameters,

$$\langle T_2 \rangle = \frac{1}{2\pi}\int_0^{2\pi} T_2(\phi_1, \phi_2)\,\mathrm{d}\theta \neq 0\,. \tag{21}$$

Otherwise stated, the average torque $\langle T_2 \rangle$ can be rendered asymmetric [8].

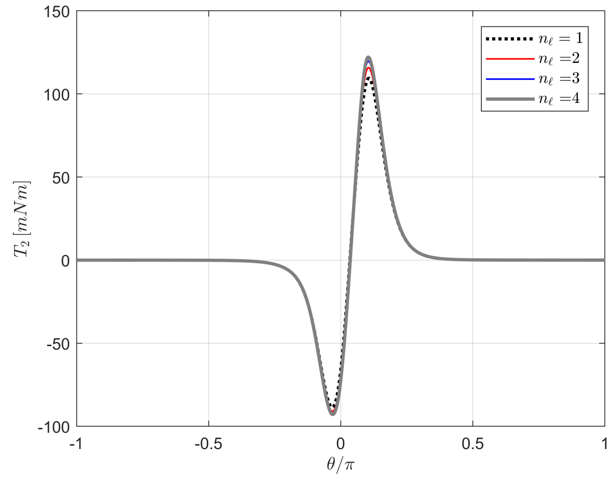

Fig. 6: Calculated static torque characteristics of a prime-mover cell with just one PM at each rotor (but keeping the radial misalignment $\phi_0 = -5^o$ between rotors, see Fig. 1). The magnets are modeled by sets of n_ℓ current loops and corresponding separation h_ℓ between loops (as in Fig. 2).

IV. Layout of the Mill

Taking into account the parameters in Table I, Fig. 6 depicts the resulting asymmetric torque profile of the prime-mover cell with only one PM per rotor (instead of 3 magnets shifted by 120^o as in Fig. 1). For the sake of comparison the PMs are modeled with different number of current loops n_ℓ, and salient numerical results are given in Table II.

TABLE I: Mill parameters and geometrical dimensions

Parameter		Value	Description	Fig.
r_{01}	[mm]	21.0	outer radius rotor #1	(1)
r_{02}	[mm]	30.0	outer radius rotor #2	
r_{g1}	[mm]	26.0	outer radius gear at side #1	
r_{g2}	[mm]	26.0	outer radius gear at side #2	
γ_0	[mm]	1.0	gap between rotors	
ϕ_0	[deg]	-5^o	angle shift between rotors	
R	[mm]	5.0	radius cylindrical PM	(2)
$\mathcal{H}$	[mm]	3.0	height cylindrical PM	
B_r	[T]	1.45	remanent flux density (NdFeB N52)	
I_M	[kA]	3.5	surface Amperian current	
n_ℓ	[-]	4	number of equivalent loops	
h_ℓ	[mm]	0.60	separation between loops	
I	[kA]	0.88	current in filamentary loop	
I_1	[kA]	0.88	current in loop #1	(3)
I_2	[kA]	0.88	current in loop #2	
R_1	[mm]	5.0	radius loop #1	
R_2	[mm]	5.0	radius loop #2	
n_c	[-]	8	number of stacked cells	(9)
h_c	[mm]	12.0	vertical separation between rotors	

It is possible to conclude from the outcomes in Table II that only marginal improvement in the numerical values can be expected for $n_\ell > 4$. Therefore, in the sequence it is assumed $n_\ell = 4$ in all calculations. Also note in Fig. 6 and from the results in Table II *a positive average torque systematically*

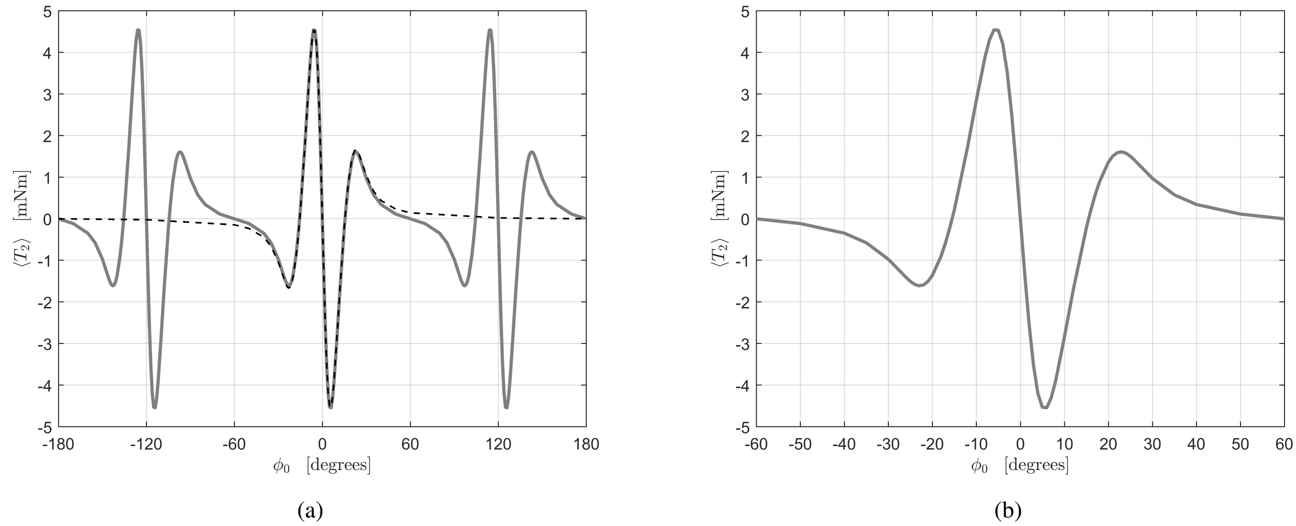

Fig. 7: (a) Calculated average torque of a prime-mover cell as function of the misalignment ϕ_0 between rotors. (b) As expected from the cell symmetry (Fig. 1), the pattern in (a) repeats at intervals of 60^o. The maximum occurs for $-6^o \leq \phi_0 \leq -5^o$. The dotted trace in (a) refers to the mean torque of a simplified cell (Fig. 6 with $n_\ell = 4$).

TABLE II: Torque values in Fig. 6

n_ℓ	[-]	1	2	3	4	# equiv loops
h_ℓ	[mm]	1.50	1.00	0.75	0.60	loop separation
$\langle T_2 \rangle$	[m Nm]	1.274	1.395	1.463	1.506	mean torque
T_2^{peak}	[m Nm]	109.4	115.8	119.6	122.1	peak torque

arises. For instance, considering $\phi_0 = -5^o$, it follows from (21) that

$$\langle T_2 \rangle_0 = 1.506\, mNm \;\approx 1.2\%\, T_2^{\text{peak}}. \tag{22}$$

In Section VI this result is considered to be significant.

The choice for $\phi_0 = -5^o$ in Fig. 6 has been decided in view of the local maxima in Fig. 7, where the mean torque as function of ϕ_0 is shown when a complete prime-mover cell with 3 PMs per rotor is considered. The detailed torque characteristics get the repeated pattern as depicted in Fig.8, where, again, $\phi_0 = -5^o$.

In Fig. 8 the average torque on the shaft becomes three times higher compared to Fig. 6, because the torque signals due to the shifted PM-pairs in Fig. 1 do not overlap. That is to say,

$$\langle T_2 \rangle_{n_c=1} = 3 \cdot \langle T_2 \rangle_0 = 4.52\, mNm. \tag{23}$$

Nevertheless, the form factor of the torque signal is still quite poor. By stacking prime-mover cells in the same shafts as show in Fig. 9, with a suitable angle shift between rotors (multiples of 45^o when $n_c = 8$), a smooth average torque is the outcome (red trace in Fig. 8), with mean value given by

$$\langle T_2 \rangle_{n_c=8} = 8 \cdot \langle T_2 \rangle_{n_c=1} = 36.2\, mNm \tag{24}$$

(see also Table III). It can be shown that above a minimum required value for cell height ($h_c = 12\, mm$ for $2R = 10\, mm$), the vertical separation between stacked rotors barely impacts the torque created by the individual cells.

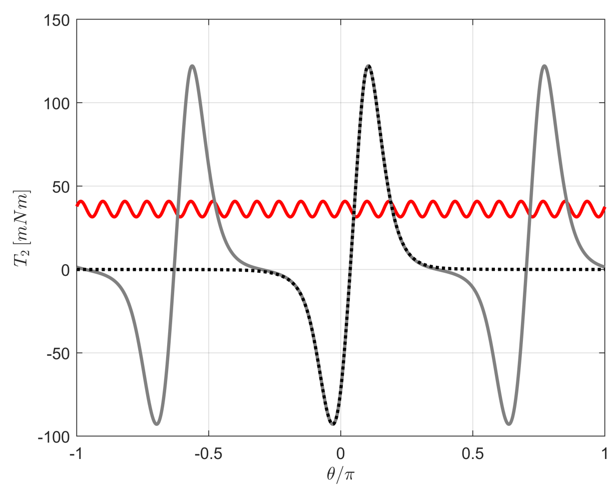

Fig. 8: Static torque profile of a prime-mover cell with 3 PM per rotor ($n_c = 1$, continued trace), and net torque profile (red trace) when stacking multiple prime-mover cells ($n_c = 8$ and $h_c = 12mm$) as sketched in Fig. 9. The dotted trace refers to the torque profile of a simplified cell (see Fig. 6.)

TABLE III: Torque values in Fig. 8

n_c	[-]	1	8	# cells
h_c	[mm]	-	12.0	cell separation
$\langle T_2 \rangle$	[m Nm]	4.52	36.2	net mean torque
T_2^{peak}	[m Nm]	122.1	40.9	peak torque

Aiming at maximizing the utilization of materials, it is opportune to interleave batteries of stacked prime-mover cells for sharing PMs, as sketched in Fig. 10, resulting a complete magnetic-wind mill. Calculations confirm that the average

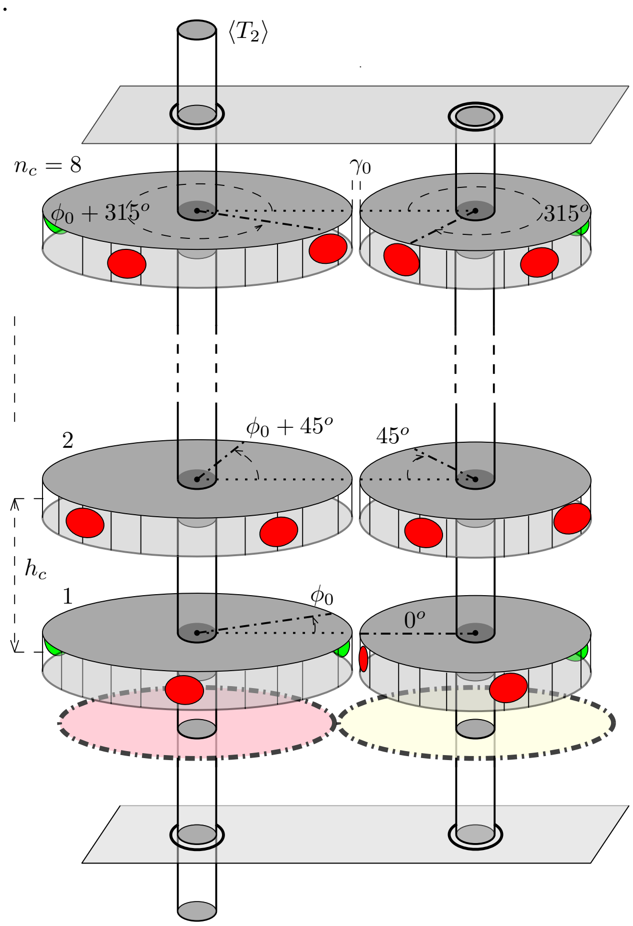

Fig. 9: Layout aiming at engineering a magnetic-wind mill that yields smooth and persistent average torque on the basis of a battery of stacked prime-mover cells.

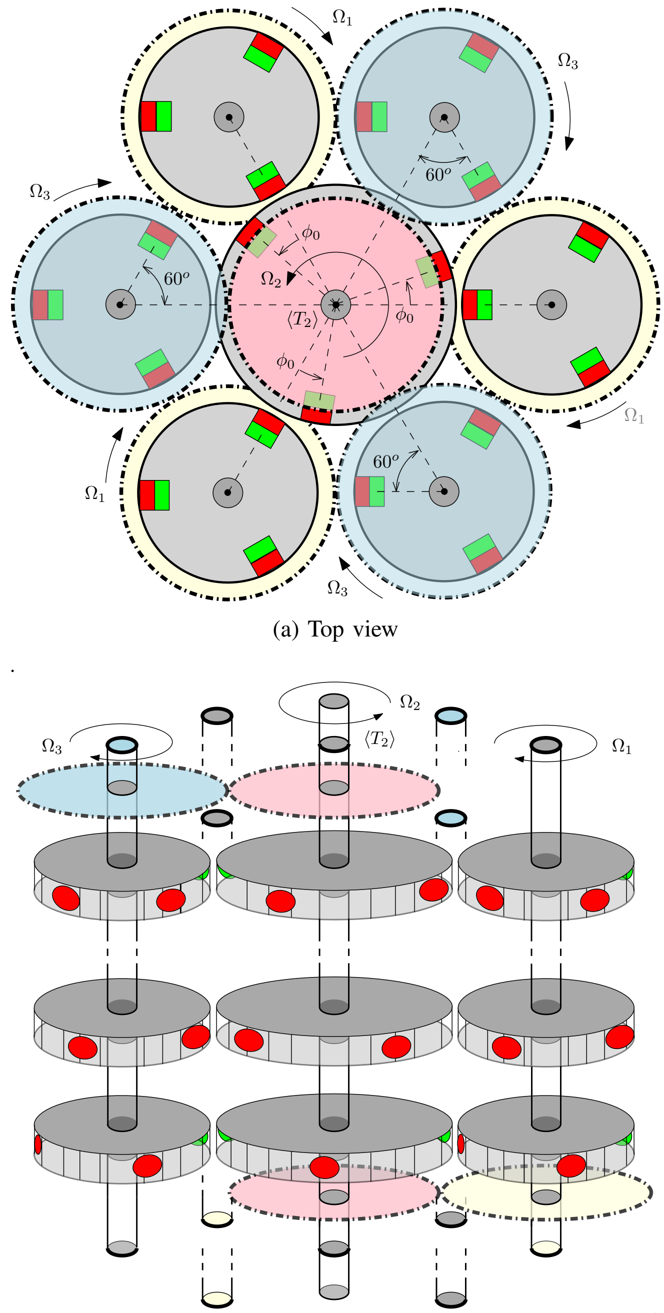

Fig. 10: Layout of a magnetic-wind mill with six interleaved bateries sharing stacked prime-mover cells, for the purpose of maximizing the utilization of the PMs. Note the subtle placement of the cog-wheels.

torque created by the extra force interaction among all PMs located in the 6 cylinders at the periphery of the mill is zero. Consequently, the final average torque on the central axis in Fig. 10 is just

$$\langle T_2 \rangle_{n_c=48} = 6 \cdot \langle T_2 \rangle_{n_c=8} = 0.217\, Nm. \tag{25}$$

The resulting torque profile is depicted in Fig. 11.

Altogether, when the central cylinder of the mill is rotating with constant radial velocity Ω_2, the average mechanical power that can be drawn from the spinning axis is found from (25) to become

$$P_2 = \Omega_2 \cdot \langle T_2 \rangle_{n_c=48}\,. \tag{26}$$

For instance,

$$\Omega_2 = 1000\, rpm \;\rightarrow\; P_2 = 22W. \tag{27}$$

It is worthwhile to remark that P_2 in (26) increases proportionally with Ω_2, since $\langle T_2 \rangle$ in (25) is found to be constant, being ideally independent of the rotational speed of the shaft, as justified in the next section.

V. Magnetic-wind mill in the field

Although the results in Fig. 11 have relation to a static situation, the torque signals may be considered without change in practical dynamic conditions. Since high-quality PM materials have a low relative permeability ($\mu_r \approx 1.03 - 1.05$ for sintered NdFeB) [1], the internal magnetization, $\vec{M}$ as given in (1), is practically not affected by the proximity of another PM with similar characteristics.

Moreover, in view of the extremely low radial speeds in mechanical devices (as the one in Fig. 10) compared to the spreading velocity of EM waves in space, the dynamic regime of the net magnetic field can be considered as quasi-stationary

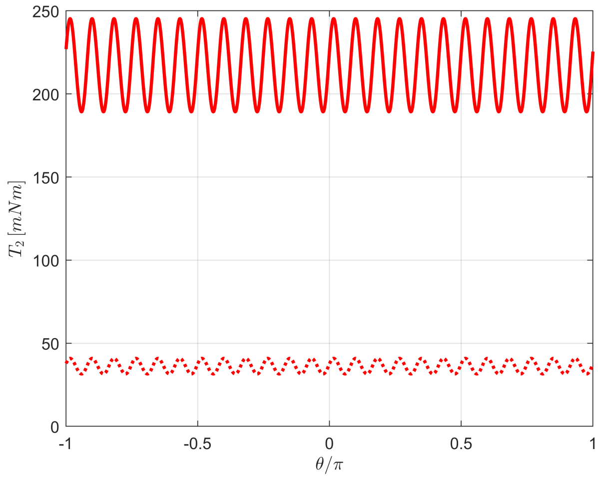

Fig. 11: Net torque characteristics of the mill sketched in Fig. 10, assembled with 6 interleaved batteries sharing prime-mover cells. The dotted trace refers to the net torque of just one battery as in Fig. 9.

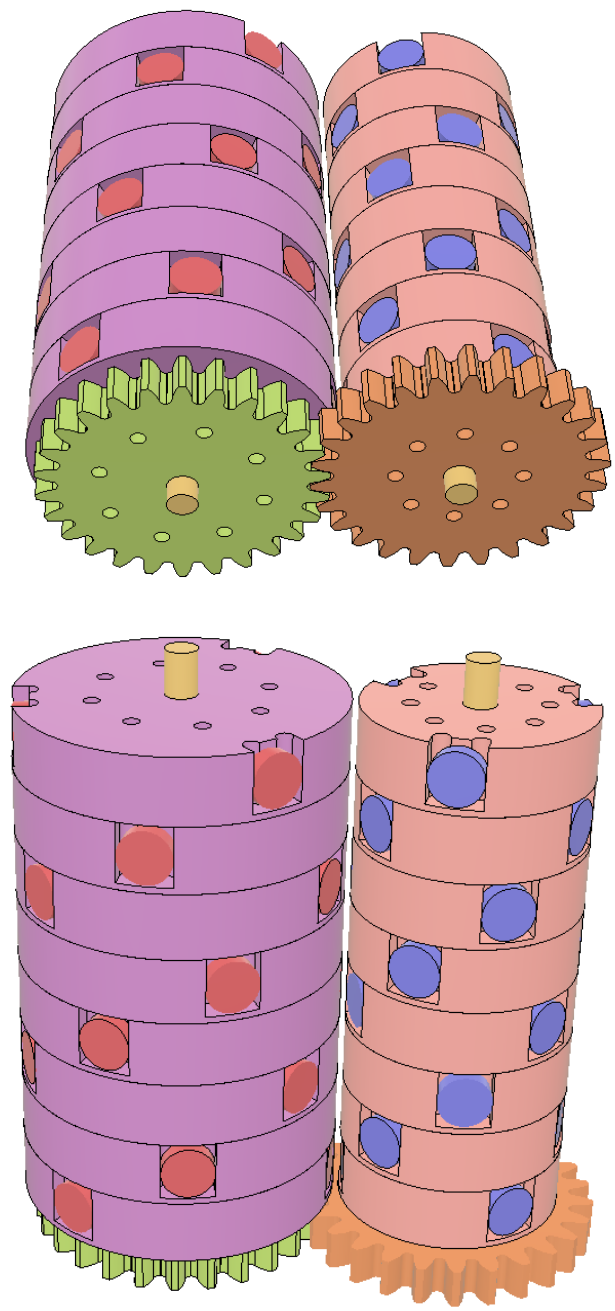

Fig. 12: Impression of mechanical parts for a mill prototype

(i.e. virtually instantaneous EM wave propagation).

Hence, from a modeling point-of-view, the currents through the filamentary loops may be assumed to remain constant, independent of the proximity of other loops, even under variable external magnetic flux. The only postulation is that $\mu_r = 1$ in- and outside the PMs.

Bearing in mind the construction of a laboratory prototype for experimental verification, Fig. 12 shows sketches of constituting parts for assembling a magnetic wind mill to operate in the field. It is expected that the maximum power that can be unfolded with the device will be limited by the vibrational stability of the mechanical part and by the induced eddy currents in the PM materials.

The PM magnetization, as such, is not directly impacted by electromotive forces (EMF) as induced by a time-changing magnetic flux due to the translation of neighbor PMs in the surrounding space. Nevertheless, by its turn this induced emf will produce eddy currents, therefore losses, in the PM material.

Magnet losses are usually neglected for plastic bonded or ferrite PMs, due to their quite high material resistivity. However, the resistivity of rare-earth magnetic materials (like NdFeB) is much lower, and eddy-current losses may increase the PM temperature to a point that the remanent magnetic flux density is noticeably affected, decreasing the PM performance as a consequence, as it is the case in high-speed PM motors [9].

VI. Discussion

Already from the beginning of the 19th century, a well-accepted model for describing the behavior of PMs can be obtained by means of *constant* electric currents circulating on the external surface of the magnetic material, the so-called Amperian currents in (3). These imaginary superficial currents are the macroscopic equivalent representation of the microscopic atomic activity of the internal particles of the material. In this way, the magnetic field as created by (a superposition of) filamentary current loops with constant current is generally accredited as a simple, yet quite effective, model for the *global* behavior of a PM, for which the magnetisation in (1) is constant all over the magnetic material.

Other PM modeling approaches for force derivation (equivalent magnetic charges, surface or volume integration of Maxwell stress tensors, scalar or vectorial formulation of virtual work principle) are also extensively used. In these representations, the formulas for calculation the total forces between PMs are quite accurate, irrespective the adopted approach. However, all above methods are only globally equivalent and do not represent the actual distribution of forces in the magnetic material, leading to specific and dissimilar results for local force density on and inside the permanent magnets [2].

It is illustrative to note the discrepancies between calculated results from different methods as compared to *accurate measurements*. A systematic and significant mismatch in the calculated torque values are clearly observed [3,Figs.3-4] [4,Fig.5], in striking contrast with the ease of obtaining precise match for calculated global magnetic forces [3,Fig.5] [5,Fig.6].

Considering the two current loops in Fig. 3 as equivalent Amperian currents in PMs, it can be proven that, if the total torque on the loops is determined by the integration of magnetic forces actuating on *local* incremental loop segments, the resulting average torque per revolution is found to become zero. Though, the spacial position of the loop segments on the PM surfaces is a mathematical abstraction without physical meaning [2]. Therefore, an appealing research question would be to try developing methods to describe *total* torques based on *global* magnetic forces, since global forces can be accurately calculated and easily measured quite well [5].

In the previous sections, a try has been done by placing the global magnetic force acting on the current loop geometric center, what could be seen as concentrating the total force on the "center of mass" of the elementary magnetic dipole moments confined by the loop. Another possibility is described in the Appendix, where the global force is placed on the point that has, on average, the highest magnetic flux density, so-called the "center of field heaviness" inside the magnetic material confined by the current loop. The magnetic flux density created by current loops at arbitrary points in space are readily and precisely calculated.

Both approaches yield similar results and bring about the challenging outcome of having the average torque per revolution not equal to zero (average torque around 1% of the peak torque value). That is to say, the tentative methods herein theoretically forecast the release of usable mechanical energy.

So, the prognostic of (41) and (42) asserts that a constrained translation of PMs (modeled as a superposition of linear loops with constant current and global forces actuating not necessarily on imaginary charges) will deploy *sustainable energy* from the sources that keep the Amperian currents constant during the trajectory. As such, the source of energy that keeps going on the microscopic atomic activity in a PM, is the same source that delivers the excess energy at every revolution of the current loops, without recurrence to any further assumption.

In Sec. 4 of [6] an interpretation is given for the energy source that propels the microscopic activity of the internal particles in a PM, resorting to elementary notions from Quantum Electrodynamics. Nevertheless, aiming at an engineering project the supposition of constant Amperian currents is enough for designing and assembling prototypes.

VII. Conclusion

A methodology for calculating global torques between PMs in close proximity is presented, being based not on incremental but global forces, avoiding in this way to assert a physical interpretation for imaginary currents. The model attempt leads to energy excess, allowing the portrayal of elementary prime-mover cells with PMs only. Subsequently, these cells are stacked to form batteries, and after that, batteries are interleaved to construct a mill in such a way that significant and persistent torque develops on the shaft to perform useful work. The next mandatory step to clarify the defiant theoretical outcomes will be, of course, to assemble a prototype with enough dexterity for conclusive experimental verification.

Appendix

Consider in Fig. 3 an arbitrary point $\vec{D}_2$ at the internal surface of current loop #2, with

$$\vec{D}_2 = u\,\vec{a}_{t2} + v\,\vec{a}_{\ell 2}\,, \tag{28}$$

where $-R_2 \leq u \leq R_2$ and $-R_2 \leq v \leq R_2$.

With respect to the reference frame placed at the geometric center of loop #1, it follows from (8) that

$$\vec{D}_{21} = \vec{C}_{21} + \vec{D}_2\,. \tag{29}$$

After some manipulations, the components of $\vec{D}_{21}$ are found to become

$$\begin{aligned} \vec{D}_{21} &= x\,\vec{a}_{t1} + y\,\vec{a}_{\ell 1} + z\,\vec{a}_{n1}\,, \text{where} \\ x &= u\cos\phi_{12} + r_2\sin\phi_{12} - \Sigma_0\sin\phi_1\,, \\ y &= -v\,, \\ z &= u\sin\phi_{12} - r_2\cos\phi_{12} + \Sigma_0\sin\phi_1 - r_1\,. \end{aligned} \tag{30}$$

The magnitude of the magnetic flux density $\vec{B}_{21}$, as induced by current loop #1 at point $\vec{D}_{21}$, is calculated with

$$|\vec{B}_{21}|(u,v) = \sqrt{B_\rho^2 + B_z^2} \tag{31}$$

in which [10]

$$B_\rho = \frac{\mu_0\,I_1\,k\,z}{4\pi\rho\sqrt{R_1\rho}}\left(-K + E\frac{R_1^2+\rho^2+z^2}{(R_1-\rho)^2+z^2}\right), \tag{32}$$

$$B_z = \frac{\mu_0\,I_1\,k}{4\pi\sqrt{R_1\rho}}\left(K + E\frac{R_1^2-\rho^2-z^2}{(R_1-\rho)^2+z^2}\right), \tag{33}$$

and

$$\rho = \sqrt{x^2+y^2}\,, \tag{34}$$

$$k^2 = \frac{4\,R_1\,\rho}{(R_1+\rho)^2+z^2}\,,\ k=\sqrt{k^2}\,, \tag{35}$$

$$\begin{aligned} K &= \int_0^{\pi/2}\frac{1}{\sqrt{1-k^2\sin^2\xi}}\,d\xi, \\ E &= \int_0^{\pi/2}\sqrt{1-k^2\sin^2\xi}\,d\xi\,. \end{aligned} \tag{36}$$

As a consequence of the intensity variations of (31) at each set of angular positions ϕ_1 and ϕ_2, the central point ($\vec{\Gamma}_2$) of the region with the highest magnetic field magnitude, circumscribed by the surface of loop #2, has changing coordinates $u_{\Gamma 2}, v_{\Gamma 2}$ given by

$$\vec{\Gamma}_2 = u_{\Gamma 2}\,\vec{a}_{t2} + v_{\Gamma 2}\,\vec{a}_{\ell 2} + r_2\,\vec{a}_{n2}\,, \tag{37}$$

where

$$u_{\Gamma 2} = \frac{\displaystyle\int_{-R_2}^{R_2} \int_{-\sqrt{R_2^2-u^2}}^{\sqrt{R_2^2-u^2}} u\,|\vec{B}_{21}|(u,v)\,dv\,du}{\displaystyle\int_{-R_2}^{R_2} \int_{-\sqrt{R_2^2-u^2}}^{\sqrt{R_2^2-u^2}} |\vec{B}_{21}|(u,v)\,dv\,du} \qquad (38)$$

and, due to symmetry, $v_{\Gamma 2} \equiv 0$. Similarly, it is possible to write for loop #1 that

$$\vec{\Gamma}_1 = u_{\Gamma 1}\,\vec{a}_{t1} + v_{\Gamma 1}\,\vec{a}_{\ell 1} + r_1\,\vec{a}_{n1}\,, \qquad (39)$$

Fig. 13 illustrates the variation range of $u_{\Gamma 1}$ and $u_{\Gamma 2}$ as function of the current loop rotation in Fig. 3. Circa $\pm 25\%$ displacement around the loop centers is found.

So, the vectors $\vec{C}_2$ and $\vec{C}_1$ defined in (9) could be interpreted as pointing to the "center of mass" of the current loops, while $\vec{\Gamma}_2$ in (37) and $\vec{\Gamma}_1$ in (39) point to the "center of field heaviness" of the loops, respectively. In this sense, it is to expect that, within the volume of PM material, the regions with higher magnetic field intensity are associated with higher force densities. Therefore, instead of (17) where

$$\vec{T}_2 = \vec{C}_2 \times \vec{F}_2 - \rho_{21}\left(\vec{C}_1 \times \vec{F}_1\right)\,,$$

an alternative moment arm for calculating the resulting torque $\vec{T}_2$ around the pivot point P_2 is given by

$$\vec{T}_2 = \vec{\Gamma}_2 \times \vec{F}_2 - \rho_{21}\left(\vec{\Gamma}_1 \times \vec{F}_1\right)\,. \qquad (40)$$

Fig. 14 depicts the resulting asymmetric static torque profile when using (40), for which holds

$$\langle T_2 \rangle = 0.730\,mNm \text{ and } T_2^{\text{peak}} = 99.4\,mNm. \qquad (41)$$

The results are quite close to the torque signal calculated with (17), also shown for comparison in Fig. 14, where

$$\langle T_2 \rangle = 1.274\,mNm \text{ and } T_2^{\text{peak}} = 109.4\,mNm. \qquad (42)$$

In both cases $\langle T_2 \rangle \approx 1.0\%\,T_2^{\text{peak}} \neq 0$!

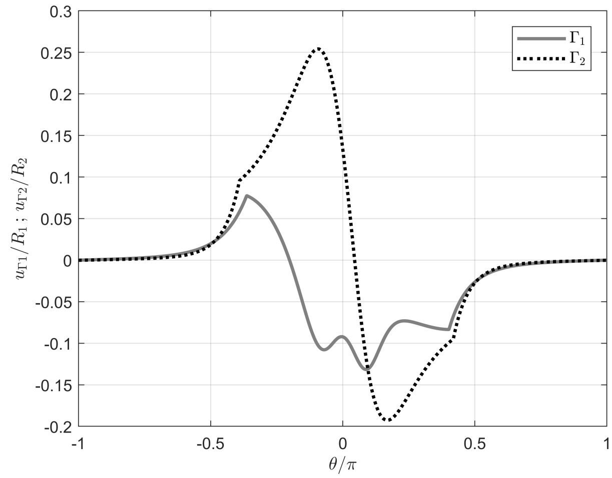

Fig. 13: Calculated displacement of $u_{\Gamma 1}$ (continuous trace) and $u_{\Gamma 2}$ (dashed trace), keeping the radial misalignment $\phi_0 = -5^o$ between current loops (corresponding to the situation when $n_\ell = 1$ in Fig. 6).

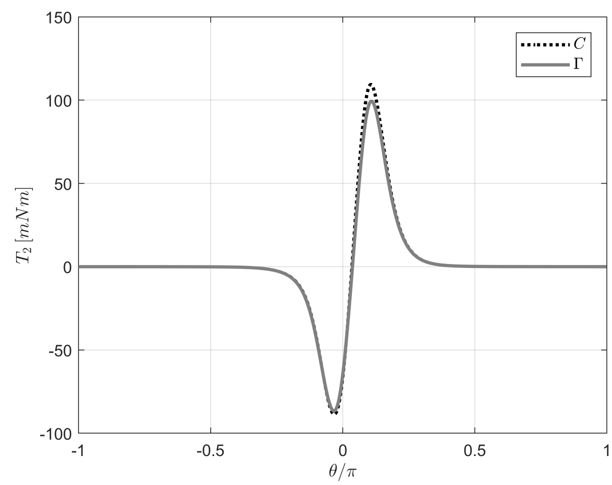

Fig. 14: Calculated static torque characteristics due to 2 current loops when taking into account the displacement of the centers of magnetic field heaviness as shown in Fig. 13 (continuous trace); and the torque signal with the magnetic forces actuating on to the loop geometric centers (dashed trace, same signal as in Fig. 6 for $n_\ell = 1$).

Acknowledgements

We would like to thank L. Kurmann, J.J. Brilman and M.A.M. Hendrix for the valuable discussions.

References

[1] E.P. Furlani. *Permanent magnet and Electromechanical Devices: materials, analysis and applications*. Academic Press, London, 6th ed., 2001.

[2] L.H. de Medeiros, G. Reyne and G. Meunieros. *About the distribution of forces in permanent magnets*. IEEE Trans. on Magnetics, vol. 35, no. 3, pp. 1215-1218, 1999.

[3] J.J. Abbott et.al. *Modeling magnetic torque and force for controlled manipulation of soft-magnetic bodies*. IEEE Trans. on Robotics, vol. 23, no. 6, pp. 1247-1252, 2007.

[4] J.L.G. Janssen et.al. *Three-dimensional analytical calculation of the torque between permanent magnets in magnetic bearings*. IEEE Trans. on Magnetics, vol. 46, no. 6, pp. 1748-1751, 2010.

[5] M.I Gonzalez. *Forces between permanent magnets: experiments and model*. Eur. J. Phys., vol. 38, 9 pp., 2017.

[6] J.L. Duarte. *Modeling the Yildiz Motor revisited*. Eindhoven University of Technology Research Report. July 2018. https://doi.org/10.6100/6b67487a-bd78-4a24-bdd1-d7b9b3dbd5b7

[7] L. Kurmann and Y. Jia, *Oscillators with Nonpolar Magnetic Repulsion System and its Use in Rotary Nonresonant and Resonant Kinetic Energy Harvesters*, IOSR J. Applied Physics, vol. 10, no. 4, pp. 57-76, 2018.

[8] L. Kurmann and J.L. Duarte. *Generation of asymmetric incommensurable torque signals*. Journal of Physics: Conference Series, [PW-17f]. POWERMEMS Int. Conf., Dec. 2018.

[9] J.L.F. van der Veen, L.J.J. Offringa and A.J.A. Vandenput. *Minimising rotor losses in high-speed high-power permanent magnet synchronous generators with rectifier load*. IEE Proc., Electr.Power Appl., vol. 144, pp. 331-337, 1997.

[10] E. Durand; *Magnétostatique*; Masson et Cie., 1968.

First appeared: February 11th, 2019 url
This version: November 11th, 2024 url

J.L. Duarte
magnetogenesis@proton.me

Essay on Magnetic-Wind Mills
Part II : Staying Power from Spacetime

J.L. Duarte
Dept. Electrical Engineering (Ret.)
Eindhoven University of Technology
The Netherlands

***Abstract*—One of the missing links in support of the allegation that devices with only magnets seemingly generate useful energy ”out of thin air” could be *Spacetime twisting*. This discussion paper applies the concept to self-rotating machines previously claimed in patents.**

I. Introduction

Classical Electromagnetism (EM) precludes the possibility of building a device that generates sustained mechanical power based solely on the attraction/repulsion of permanent magnets (PMs) [1]. However, in the periphery of Science many inventions concerning allegedly self-running magnet machines have been reported for decades. There are so many of them that specific PCT identification labels[1] are warranted. By contrast, in the eyes of mainstream Physics such inventions are dismissed as symptoms of a fascinating human obsession with *Perpetua Mobilia*[2].

Nevertheless, a newly developed extension of Einstein’s general relativity theory, called ECE (Einstein-Cartan-Evans) theory [2], provides a foundation for understanding magnet-only prime-movers.

In the next sections three self-rotating magnet motor candidates are analyzed in the context of ECE theory. Conditions for induction of resonance in ambient spacetime are shown, which, according to [2], could explain the transfer of energy from spacetime itself to the device, thus creating a steady flow of mechanical power.

II. Self-running machines

The first device is the subject of a patent filed in Brazil in 1989 [5], so it can be considered disclosed prior-art in present time. The inventor proposes a base magnetic assembly as shown in Fig. 1, and claims that when stacking and interleaving a few sets around a rotatable central shaft (label ***2*** in Fig. 1) the device exhibits self-running behavior and becomes a prime-mover.

In Fig. 1, the PMs on the rotor and stator are located in sockets (***3*** and ***4***, respectively). The stator sockets are in line with the rotor ones, both with the same angular displacement (angle α) referenced to the rotor radius.

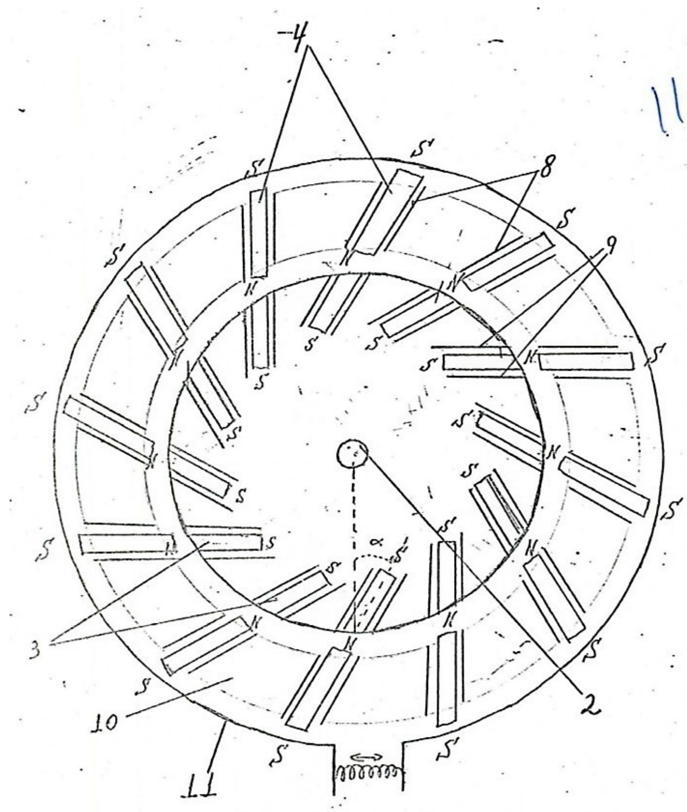

Fig. 1: Original drawings of a magnet-only base assembly as given in [5], consisting of rotor and stator with PMs embedded in sockets. By stacking and interleaving such base sets around a shaft, the resulting device would behave as an autonomous prime-mover.

The displaced angle α is intended to soften sharp transitions from repulsive to attractive magnetic forces while spinning. Moreover, for further improvement of motor performance, it is also advised to include socket linings of ferromagnetic material (***8*** and ***9***), such that the PMs are partially screened and, therefore, the resulting magnetic field becomes more longitudinally focused.

It is stated in [5] that the gap depth between stator and rotor magnets allows steering the rotation speed. For this purpose, and to avoid expulsion during operation, the stator PMs are retained in open sockets (***10*** in Fig. 1) by means of an

[1] *H02K 53/00, H02N 11/00*

[2] Counting from 2015 onwards, PatBase shows 3100 patent families of genuine alleged perpetual motion machines.

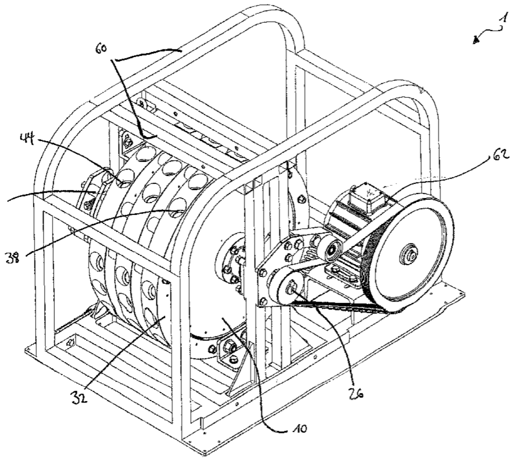

Fig. 2: Magnet-only machine as claimed in [6], consisting of PMs embedded in sockets and fastened by locking pins.

adjustable exterior metal belt (label ***11***). As such, the stator magnets are not firmly attached, and consequently they will somehow vibrate mechanically during operation (a feature not evidenced in the patent). In particular, these vibrations must be explicitly taken into account with respect to ECE theory, because magnetic harmonic oscillations, even of quite limited magnitude, are the key to generating resonance in spacetime, as explained in the next section.

Unfortunately, no verifiable record has been found whether an engine prototype based on [5] has been effectively demonstrated to work. Still, it is an intriguing situation when compared to another patent filed in Germany in 2004 [6].

Fig. 2 shows the self-running motor in [6], which is strikingly similar to the one in [5], although [5] is not mentioned in the prior-art search report of [6]. The subtle difference in [6] is that, in order to hold the PMs in place and prevent them for driven out of the sockets during operation, the rotor and stator magnets contain a locking pin through transversal holes. So, as with [5], the PMs are not sturdily fastened. With an inferior fit between locking pins and transversal holes, (tiny) mechanical vibrations inevitably occur during rotation.

Perhaps the use of tighter locking pins is the reason why the inventor in [6] was unable to reproduce the operation of the device in later implementations, despite some successful public demonstrations with earlier prototype versions (so goes the well-known story about the *Perendev project*). Being unaware of the essential need for small mechanical vibrations (nothing about this is mentioned in [6]), it could be that in later prototypes the mounting of PMs in sockets with pins had been "much improved", nullifying the vibrations (with tragic legal consequences).

In 2022, another Brazilian inventor posted a series of videos on YouTube showing self-running magnet motors in full operation [7]. These devices are simplified realizations of [5] and [6]'s ideas. Interestingly, the required magnetic vibrations appear due to the flexible materials used to construct the motors. The videos show self-sustaining and stable rotation, while the motor parts are transparently dissected to show their internal contents.

Continuing along the path of high expectations initiated in Part I of this essay [8], a qualitative analysis of the possible origin of the mean torque that would lead to auto-rotation in the above inventions is conducted further in the framework of ECE theory.

III. Resonance in spacetime

Stacking identical base assemblies as outlined in Fig. 1 around a common shaft, while interleaving the base assemblies with a constant angular offset, produces an overall cylindrically shaped package. The resulting magnetic field in the region between rotor and stator will present circularity. To a first approximation, the radial part of the magnetic flux density, $\vec{B}$, can be described as a circularly polarized plane wave given by

$$\vec{B} = B\left[\cos(\kappa z - \omega t),\, \sin(\kappa z - \omega t),\, 0\right]\begin{bmatrix}\hat{e}_x\\ \hat{e}_y\\ \hat{e}_z\end{bmatrix} \tag{1}$$

where B (in Tesla) has constant magnitude and $\{\hat{e}_x, \hat{e}_y, \hat{e}_z\}$ are orthonormal Cartesian vectors, with $\hat{e}_z$ aligned with the longitudinal shaft in the cylindrical assembly. In (1) the value of wave-number κ is found from the dimensions of the base assembly, together with the amount of stacked base sets in conjunction with the applied interleaving angle, and ω denotes the angular frequency of the rotating shaft.

It is usual practice in classical EM to describe the magnetic field $\vec{B}$ with the aid of a vector potential $\vec{A}$ as

$$\vec{B} = \vec{\nabla} \times \vec{A} \;\text{ and }\; \vec{\nabla} \cdot \vec{A} = 0 \tag{2}$$

Accordingly, it is found from (1) and (2) that

$$\vec{\nabla} \times \vec{A} = -\kappa \vec{A} \tag{3}$$

That is to say, the potential $\vec{A}$ in (3) has characteristics of a Beltrami flow[3] (and consequently also $\vec{B}$ in (1)).

The back-and-forth movement of the stator PMs due to the approach and subsequent depart of the spinning rotor magnets produces an additional, pulsed component in the magnetic flux density in the region between rotor and stator. Using the same orthonormal basis in (1), the first-harmonic approximation of the magnetic pulses in the radial direction is obtained with

$$\vec{B}_0 = B_0 \cos(\omega t + \varphi)\left[\cos(\kappa_0 z),\, \sin(\kappa_0 z),\, 0\right]\begin{bmatrix}\hat{e}_x\\ \hat{e}_y\\ \hat{e}_z\end{bmatrix} \tag{4}$$

where the magnitude B_0 (in Tesla) and the phase shift φ are functions of the displaced angle $\boldsymbol{\alpha}$. Furthermore, since the stator parts follow the same stacking and interleaving pattern as the rotor parts, it results equal values for the spatial frequencies κ and κ_0. Otherwise stated, by construction

$$\kappa_0 = \kappa \tag{5}$$

It should be noted that the harmonic oscillations of $\vec{B}_0$ are perfectly synchronized with the angular frequency ω of $\vec{B}$ in

[3]Flows in which the velocity vector $\vec{v}$ and the vorticity vector $\vec{\nabla} \times \vec{v}$ are parallel to each other.

(1). The reason for this is that the rotor and stator magnets attract/repel each other at the same rate given by the angular frequency ω of the rotor.

Similarly to (2), a vector potential $\vec{A}_0$ associated with $\vec{B}_0$ is found from (4) as

$$\vec{B}_0 = \vec{\nabla} \times \vec{A}_0 = -\kappa_0 \vec{A}_0 \tag{6}$$

ECE theory deals with magnetogenesis, and states that magnetic field may be generated from torsion in spacetime [2]. In this section, we track [3] and [4].

Magnetic flux density as created from spacetime is describe in its simplest form by

$$\vec{B}_S = \vec{\nabla} \times \vec{A}_S - \vec{\varpi} \times \vec{A}_S \tag{7}$$

where $\vec{\varpi}$ is a spin connection vector to twisting in spacetime. The subscript S in (7) is introduced to emphasize quantities generated by the spacetime, not by the magnetic assembly itself. In case of a potential $\vec{A}_S$ consisting of circular plane waves, $\vec{\varpi}$ gets a special form leading to

$$\vec{\varpi} \times \vec{A}_S = -\kappa \vec{A}_S \tag{8}$$

and (7) is found to become

$$\vec{B}_S = \vec{\nabla} \times \vec{A}_S + \kappa \vec{A}_S \tag{9}$$

The spatial frequency κ in (9) is a quantity imposed by the magnetic geometry of the assembly, as before, and, to stress it again, the quantities $\vec{A}_S$ and $\vec{B}_S$ are properties of spacetime itself where the assembly is located.

Under equilibrium conditions, the spacetime around the magnetic assembly produces no magnetic flux, hence $\vec{B}_S = 0$. In this case, given (9),

$$\begin{aligned} \vec{\nabla} \times \vec{B}_S &= 0 \\ \vec{\nabla} \times (\vec{\nabla} \times \vec{A}_S) + \vec{\nabla} \times (\kappa \vec{A}_S) &= 0 \\ \vec{\nabla}(\vec{\nabla} \cdot \vec{A}_S) - \nabla^2 \vec{A}_S - \kappa^2 \vec{A}_S &= 0 \end{aligned} \tag{10}$$

Since for circular plane waves $\vec{\nabla} \cdot \vec{A}_S = 0$, it results from (10) that

$$\left(\nabla^2 + \kappa^2\right) \vec{A}_S = 0 \tag{11}$$

Overall, (11) is a Helmholtz equation that defines equilibrium conditions in the spacetime around the magnetic assembly, when there is no Cartan torsion and therefore no external magnetic field generation. Consequently, there is no spacetime related torque to rotate the magnetic assembly.

Torque can be create by disturbing the Beltrami flow, which means the equilibrium at zero in (11) must no longer be fulfilled. In this context, the ECE theory forecasts that a periodic imbalance may disturb the structure of the ambient spacetime [4]. Under disturbances, (11) is then transformed to an undamped resonator with a driving term.

In this report, we assume further that the oscillations introduced in spacetime by the pulsed potential $\vec{A}_0$ given in (6) modifies (11) by adding a right-hand term as

$$\left(\nabla^2 + \kappa^2\right) \vec{A}_S = \gamma \vec{A}_0 \tag{12}$$

for some value of γ.

From the general form in (12), the Cartesian components of $\vec{A}_S$, say $\{A_{Sx}, A_{Sy}, A_{Sz}\}$, are readily found. For instance, after manipulations with (4) and (6), it follows from (12) that

$$\frac{\partial^2 A_{Sx}}{\partial z^2} + \kappa^2 A_{Sx} = \gamma A_0 \cos(\omega t + \varphi) \cos(\kappa_0 z) \tag{13}$$

for which the solution is found to become

$$A_{Sx} = \frac{\gamma}{(\kappa^2 - \kappa_0^2)} A_0 \cos(\omega t + \varphi) \cos(\kappa_0 z) \tag{14}$$

On account of (5), the resonance introduced by disturbance $\vec{A}_0$ will induce the vector potential component A_{Sx} to grow towards infinity, even for quite small values of γ in (14). As a result, an external magnetic field, $\vec{B}_S$, is created from spacetime around the magnetic assembly, which gives rise to a torque on the PM magnetic moments $\vec{m}$ as

$$\vec{T}_S = \vec{m} \times \vec{B}_S \,, \tag{15}$$

with $\vec{T}_S$ high enough to make the shaft rotate.

Finally, the energy flow required to keep rotation going presumably comes from the resonance interactions with the chaotic and abundant vacuum energy, ubiquitously available in spacetime [2] [8].

IV. Conclusion

This discussion paper makes a link between (unintended) PM mechanical vibrations and the power output of patented devices. ECE's theory explicitly states that useful energy can be obtained from spacetime via this framework. The theory points to the opening of an energy gateway, and could provide a basis for development and engineering of self-running machines. *Is it too good to be true?* Further experiments with previously disclosed inventions may lead to a clear answer to this research question.

References

[1] E.P. Furlani, *Permanent magnet and Electromechanical Devices: materials, analysis and applications*. Academic Press, London, 6th ed., 2001

[2] H. Eckardt, *Einstein-Cartan-Evans Unified Field Theory - The Geometrical Basis of Physics* (textbook), 2022, Paper 438, UFT section www.aias.us

[3] M.W. Evans and H. Eckardt, *Spin connection resonance in magnetic motors*, Physica B 400, 2007, pp. 175-179

[4] H. Eckardt, *How do space energy devices work?*, 2007, http://aias.us/documents/miscellaneous/SpaceEnergy.pdf

[5] M.C. Malafaia, *Motor magnetico*, PI 8900294 A, Brazilian patent office INPI, Aug 1990, (in Portuguese)

[6] M. Brady, *Permanent magnet machine*, WO 2006/045333 A1

[7] *Dicas do Leao*, https://www.youtube.com/watch?v=pMD-GSjqqmc https://www.youtube.com/watch?v=IBV8Pg0RcII

[8] J.L. Duarte,*Essay on magnetic-wind mills - Part I analysis and design*, TU Eindhoven Research Report, Feb 2019, doi.org/10.6100/94FC4756-AC0A-4A9C-A1DD-58530E694BB8

*First appeared: November 15th, 2022*url
*This version: November 11th, 2024*url

J.L. Duarte
magnetogenesis@proton.me

Essay on Magnetic-Wind Mills Part III : Pathway for energy transfer

J.L. Duarte
Dept. Electrical Engineering (Ret.)
Eindhoven University of Technology
The Netherlands

***Abstract*—An attempt is made to describe that mechanical vibrations are not only responsible for evoking spacetime resonances, as Einstein-Cartan-Evans theory predicts, but could also provide a possible interface for transferring energy from the quantum vacuum to a rotating shaft.**

I. INTRODUCTION

The assembly around a magnetic-wind mill, presented in [1], may appear unusual at first glance. However, it essentially serves as a practical experimental setup for investigating a process of scavenging energy from the quantum vacuum, as outlined by the ECE theory [2].

The inventor in [1] claims that the magnetic mill generates useful output power in the kilowatt range. Additionally, it is worth noting that this assembly represents an evolution of earlier work involving transparent, fully open, low-power prototypes [3][1].

As a sequel to [4], analysis of [1] is advanced in the present paper, with the aim of evaluating if mechanical vibrations could provide a means of transferring energy to the mill shaft.

We start in Section II by reviewing the setup assemblage. In Section III, we derive expressions for the global forces actuating on the magnets, on the basis of an extended Lorentz Force law that takes elementary magnetic dipole moments into account. Next, owing to the low rigidity of the assembled structure, we show in Section IV that the rotor angular vibrations, which are dynamically generated proportionally to radial force acceleration, could add net mechanical energy to the rotating parts. Finally, we conclude the analysis in Section V, including a numerical example to verify that the calculated rotor angular vibrations have realistic small values, as expected.

II. A PECULIAR EXPERIMENTAL SETUP

The flux mill in [1] has a hollow cylindrical rotor that is assembled from a thin-metal can, and a hinge-like split stator surrounding the rotor. On the rotor's surface, 64 PM disks (short cylindrical-shaped permanent magnets) are fixed in helix staggering (4 rings with 16 magnets per ring). The 2-part stator has also 64 magnets in total (4 rings per part, 8 magnets per split ring), facing the rotor magnets with the same magnetic polarity.

[1]The results obtained in this paper are also relevant for [3].

The two parts of the stator are joined together by a non-rigid clip, which leads to small mechanical vibrations during operation. All magnet disks have the same dimensions (5mm/2mm), with some iron filings around to facilitate crossing when magnets meet during rotation. Moreover, a flywheel is added to the rotor shaft to smooth rotational speed.

As sketched in the Appendix, the flux mill shaft is mechanically driven by a belt coupled to the shaft of a 127VAC single-phase motor (washing-machine motor type). This motor is electrically fed by one of the two AC outlets of a DC/AC power electronic inverter (from 12V DC to 110V/60Hz square-wave AC).

In turn, the electronic inverter's 12VDC inlet is powered by the rectified DC voltage from an alternator (a automobile starter motor/generator), while a 12V battery is also linked in parallel to the same DC contacts. Finally, the alternator's shaft is also belt-coupled to the flux mill shaft.

Altogether, we have a loop concerning energy circulation, where the expected prime-mover is the magnetic flux mill.

To begin with operation, the electronic inverter DC voltage is set by the 12V battery, in order to bring all the shafts up to nominal speed (as in an automobile). Subsequently, the battery cables are disconnected. From this moment on, there are no other conventional sustainable power sources in the setup.

After reaching stable operation, a variety of loads are connected to the electronic inverter's second AC outlet (like light bulbs, drills, electric saw, etc.), and enough energy is unfolded, as shown in the video.

Given the "vibrational" approach stated in [4], there should be an additional, exterior magnetic field in the environment of the flux mill, other than the own magnetic fields created by the stator and rotor magnets.

This external B field is evoked from spacetime resonances, and has a circularly polarized flux density waveform with general expression (in ccw convention):

$$\vec{B}_{ext} = B_S \left[\cos(\kappa z - \omega t)\vec{a}_x - \sin(\kappa z - \omega t)\vec{a}_y \right], \qquad (1)$$

where $\vec{a}_x, \vec{a}_y$ are orthonormal vectors referenced to a stationary frame, and ω the rotor shaft angular velocity. In the case of a rotor with radius r_C and height h_C, where n equally separated rings with η magnets per ring are inlaid, the wavenumber κ in (1) is found to become

$$\kappa = \frac{n-1}{\eta} \, \frac{\pi}{h_C}. \qquad (2)$$

III. (NON)CONSERVATIVE MAGNETIC FORCES

Fig. 1 shows a situation in which a magnetic dipole moment that represents a PM disk, $\vec{\mu}_C$, is attracted/repelled by an external magnetic field, $\vec{B}_{\text{ext}}\,[T]$, wherein the disk is moved. As a result, work will be done in the process.

The center coordinates of the magnet disk are referenced to orthonormal vectors $(\vec{a}_x, \vec{a}_y, \vec{a}_z)$, together with associated radial and rotational vectors

$$\begin{aligned}\vec{a}_r &= \cos\phi\,\vec{a}_x + \sin\phi\,\vec{a}_y, \\ \vec{a}_\phi &= -\sin\phi\,\vec{a}_x + \cos\phi\,\vec{a}_y,\end{aligned} \tag{3}$$

according to the convention for rotation angle ϕ.

In permanent magnets, the magnetic field arises from intrinsic elementary spin dipole moments in the material [5]. As such, the PM disk is assumed to have homogeneous volumetric density of magnetic dipole moments, $M\,[Am^2/m^3]$, with $M = B_{\text{re}}/\mu_0$, where $B_{\text{re}}\,[T]$ is the remanent magnetization of the material, and $\mu_0 = 4\pi 10^-7\,[H/m]$ the permeability of free space.

Further, as an approximation, we also consider that in a spacial disk volume, the external B field has approximately the same value as at the center. Consequently, a PM disk, with radius R_D and height h_D, is modeled as single dipole moment, $\vec{\mu}_C$, which represents the superposition of all elementary spin dipole moments in the disk volume pointing out in the same direction, with

$$\parallel \vec{\mu}_C \parallel = \mu_C = \pi R_D^2 h_D M. \tag{4}$$

In Fig. 1, $\vec{\mu}_C$ with coordinates (x_C, y_C, z_C) is free to rotate with constant radius r_C and angular displacement ϕ around the axis $\vec{a}_z$. That is to say,

$$\begin{aligned}x_C &= r_C\cos\phi\,, \\ y_C &= r_C\sin\phi\,,\end{aligned} \tag{5}$$

and

$$\vec{\mu}_C = \mu_C\,\vec{a}_r\,. \tag{6}$$

Superposed to ϕ, small angular disturbances, ϕ'_S in Fig. 1, take place, representing shaft angular vibrations, which arouse when a rotor magnet crosses the stator magnets in proximity, as considered later.

According to [5], in order to analyze the interaction between the dipole moment $\vec{\mu}_C$ and the field $\vec{B}_{\text{ext}}$, the classical Lorentz Force formula has to be extended with one more component as

$$\vec{F} = q\vec{E}_{\text{ext}} + q\vec{v}\times\vec{B}_{\text{ext}} + \vec{\nabla}(\vec{\mu}_C\cdot\vec{B}_{\text{ext}}). \tag{7}$$

The term $\vec{\nabla}(\vec{\mu}_C\cdot\vec{B}_{\text{ext}})$ is capable of performing work, what is not the case for $q\vec{v}\times\vec{B}_{\text{ext}}$.

A research question in this discussion paper is, if the magnetic force introduced by the $\vec{\nabla}(\vec{\mu}_S\cdot\vec{B}_{\text{ext}})$ term is *conservative*. It will be the case if there is zero net work done when moving the dipole moment $\vec{\mu}_C$ through the field $\vec{B}_{\text{ext}}$, following the closed cyclic path $0 \leq \phi \leq 2\pi$. If *not*, then net energy will be taken from the external magnetic field.

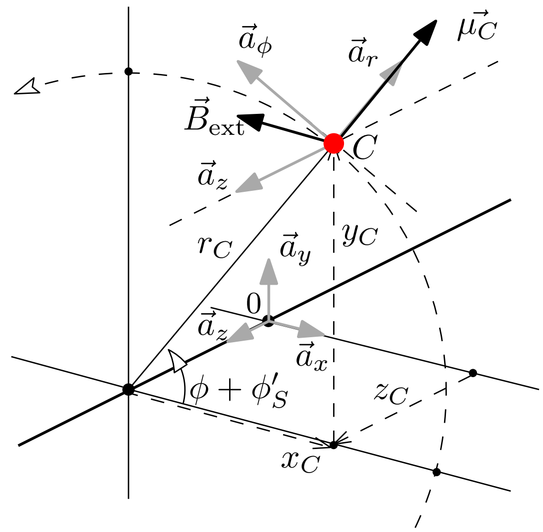

Fig. 1: Magnetic dipole moment, $\vec{\mu}_C$, which models a PM disk in rotational motion with angle ϕ and constant radius r_C, through an external magnetic field, $\vec{B}_{\text{ext}}$. Small angular disturbances, ϕ'_S, are also present.

IV. MECHANICAL VIBRATIONS MEET MAGNETIC OSCILLATIONS

As previously mentioned, a circularly polarized magnetic flux density waveform is assumed for the external B field, which is generated by spacetime resonances.

Essentially, due to the low rigidity of the mill frame, there is an oscillation of the radial distance between rotor and stator magnets and therefore of the force between them. Hence, the own magnetic fields created by the rotor and stator magnets, and, consequently, also the external B field, are slightly distorted by mechanical vibrations. This oscillation contains any harmonics of the rotation frequency, but for sake of simplicity we restrict to the ground frequency.

So, in the sequence, we consider that the external B field is radial in direction[2] and varying with the angle ϕ, the angle of the rotational motion of the rotor magnets. Since the stator magnets are distinct, there should also be angular components, although symmetric to the positions of the magnets. Anyway, these angular components are neglected, because they do not contribute to the net rotational force[3].

Therefore, as an extension of (1), the external B field at (x_C, y_C, z_C) is described by

$$\vec{B}_{\text{ext}} = B_{\text{ext}}\left[\cos\phi\,\vec{a}_x + \sin\phi\,\vec{a}_y\right]\,, \tag{8}$$

with $\phi = \omega t - \kappa z_C$, while

$$B_{\text{ext}} = B_S + B'_S\cos(\eta\phi), \tag{9}$$

where B_S and B'_S are constant, and $B'_S \ll B_S$.

The term $B'_S\cos(\eta\phi)$ in (9) is a first-order approximation for the field magnitude oscillations, when $\vec{\mu_C}$ (that models one rotor magnet) cyclically crosses over η stator magnets in a ring, for $0 \leq \phi \leq 2\pi$.

[2] i.e., $\vec{B}_{\text{ext}} = B_{\text{ext}}\,\vec{a}_r$, with variable B_{ext}.

[3] Angular components in $\vec{B}_{\text{ext}}$ are *tangential* to $\vec{\mu}_C$, vanishing in (7).

Without loss of generality, $z_C \equiv 0$ is chosen for (8), meaning that the focus is just in one of the stator magnet rings.

A. Magnetic force components

Defining

$$\mathcal{F} = \vec{\mu}_C \cdot \vec{B}_{\text{ext}}, \tag{10}$$

it follows from (6) and (8) that

$$\mathcal{F} = \mu_C \left(B_S + B'_S \cos(\eta\phi) \right). \tag{11}$$

Correspondingly, the resulting force on the magnetic dipole moment $\vec{\mu}_C$ is obtained with reference to (7) :

$$\vec{F}_C = \vec{\nabla}\mathcal{F}. \tag{12}$$

The required gradients in (12) can be calculated as function of the rotation angle ϕ with

$$\vec{F}_C = \frac{\partial\mathcal{F}/\partial\phi}{\partial x_S/\partial\phi}\vec{a}_x + \frac{\partial\mathcal{F}/\partial\phi}{\partial y_S/\partial\phi}\vec{a}_y, \tag{13}$$

where, from (11),

$$\frac{\partial\mathcal{F}}{\partial\phi} = -\eta\mu_C B'_S \sin(\eta\phi), \tag{14}$$

and, in regard to (5),

$$\begin{aligned} \partial x_S/\partial\phi &= -r_C \sin\phi, \\ \partial y_S/\partial\phi &= r_C \cos\phi. \end{aligned} \tag{15}$$

Respecting cylindrical coordinates, $\vec{F}_C$ is given by

$$\begin{aligned} \vec{F}_C &= F_r\,\vec{a}_r + F_\phi\,\vec{a}_\phi, \\ F_r &= F_x \cos\phi + F_y \sin\phi, \\ F_\phi &= -F_x \sin\phi + F_y \cos\phi. \end{aligned} \tag{16}$$

After substitution of (15) into (13), it follows from (16) that

$$\begin{aligned} F_r &= \frac{\partial\mathcal{F}}{\partial\phi}\,\frac{\cos\phi}{-r_C\sin\phi} + \frac{\partial\mathcal{F}}{\partial\phi}\,\frac{\sin\phi}{r_C\cos\phi} \\ &= -\frac{2}{r_C}\frac{\partial\mathcal{F}}{\partial\phi}\frac{\cos(2\phi)}{\sin(2\phi)}, \end{aligned} \tag{17}$$

$$\begin{aligned} F_\phi &= -\frac{\partial\mathcal{F}}{\partial\phi}\,\frac{\sin\phi}{-r_C\sin\phi} + \frac{\partial\mathcal{F}}{\partial\phi}\,\frac{\cos\phi}{r_C\cos\phi} \\ &= \frac{2}{r_C}\frac{\partial\mathcal{F}}{\partial\phi}, \end{aligned} \tag{18}$$

which leads to, in view of (14),

$$F_r = F_0\frac{\sin(\eta\phi)\cos(2\phi)}{\sin(2\phi)}, \tag{19}$$

$$F_\phi = -F_0\sin(\eta\phi), \tag{20}$$

with

$$F_0 = 2\frac{\eta\mu_C B'_S}{r_C}. \tag{21}$$

A plot of (19)-(20) for $\eta = 16$ is shown in Fig. 2. It can be seen that the magnet assembly geometry brings about impulsive acceleration for the radial forces[4].

[4]Asymptotic behaviour of (19).

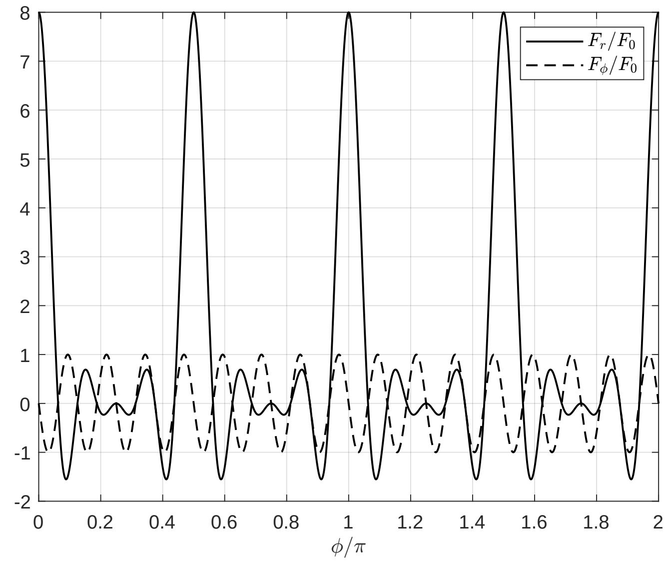

Fig. 2: Radial (F_r) and rotational (F_ϕ) forces. Normalized Eqs.(19)-(20) with $\eta = 16$.

B. Rotor angular vibration

The vibrating rotational angle, ϕ'_S in Fig. 1, is due to the superposition of a variety of mechanical perturbations. Be that as it may, a primary assumption in this paper is to consider that ϕ'_S has a component that is *dynamically* aroused by the acceleration of *radial forces* in the flux mill.

Therefore, since stator and rotor radial forces are similar, an expression for infinitesimal increments of ϕ'_S is written as

$$d\phi'_S = \lambda\frac{\partial F_r}{\partial\phi}d\phi, \tag{22}$$

where λ is a constant of proportionality, intrinsic to the assemblage mechanical rigidity, and, with reference to (19),

$$\frac{\partial F_r}{\partial\phi} = -F_0\left[2\frac{\sin(\eta\phi)}{\sin^2(2\phi)} - \eta\frac{\cos(\eta\phi)\cos(2\phi)}{\sin(2\phi)}\right]. \tag{23}$$

A plot of (23) for $\eta = 16$ is illustrated in Fig. 3.

Owing to (22), the vibrating rotational angle is determined with

$$\phi'_S = \lambda\int\frac{\partial F_r}{\partial\phi}d\phi\,, \tag{24}$$

and its peak-to-peak magnitude, $\Delta\phi'_S$, ascertained from

$$\Delta\phi'_S = \max(\phi'_S) - \min(\phi'_S)\,,\; 0 \le \phi \le 2\pi. \tag{25}$$

C. Energy increments

Work is done by F_ϕ, the angular force component in (20), upon the dipole moment $\vec{\mu_C}$ at each linear increment $d\phi'_S$. Since $\vec{\mu_C}$ is located with radius r_C around a pivot axis, a infinitesimal energy increment equal to

$$dQ'_S = F_\phi\, r_C\, d\phi'_S \tag{26}$$

is, therefore, added to the rotating system parts.

In relation to (18) and (22), (26) is found to become

$$dQ'_S = 2\lambda\left(\frac{\partial\mathcal{F}}{\partial\phi}\right)\left(\frac{\partial F_r}{\partial\phi}\right)d\phi. \tag{27}$$

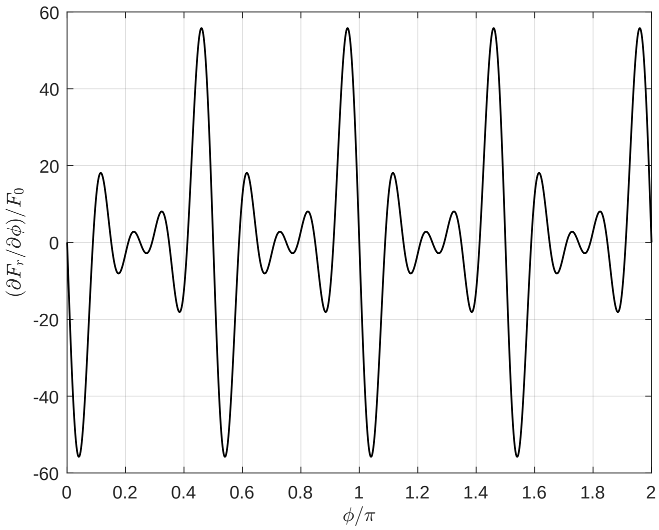

Fig. 3: Rate-of-change of the radial force in Fig.(2). Normalized Eq.(23) with $\eta = 16$.

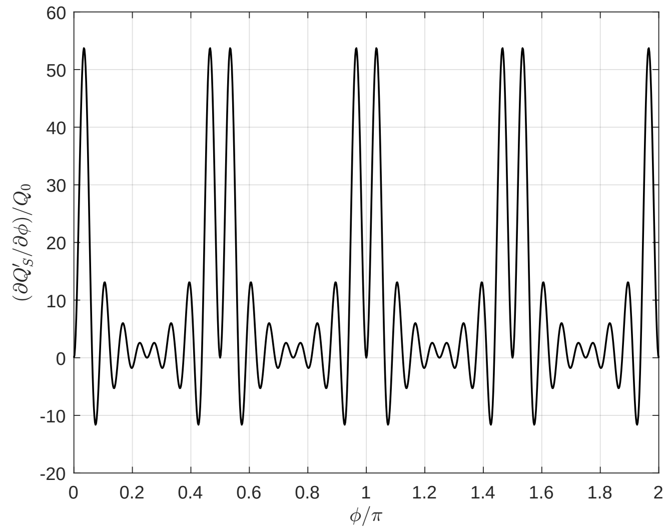

Fig. 4: Oscillations in energy transfer as function of the shaft angular position. Normalized Eq.(28) with $\eta = 16$.

Taking (14) and (23) into account, after some manipulations it results from (27) that

$$\frac{\partial Q'_S}{\partial \phi} = Q_0 \frac{\sin(\eta\phi)}{\sin(2\phi)} \left[2\frac{\sin(\eta\phi)}{\sin(2\phi)} - \eta\cos(\eta\phi)\cos(2\phi) \right] \quad (28)$$

with

$$Q_0 = 8\frac{\lambda(\eta\mu_C B'_S)^2}{r_C} \,. \quad (29)$$

A plot of (28) for $\eta = 16$ is shown in Fig. 4. It can be seen that the average of $\partial Q'_S/\partial\phi$ is not zero. Asymmetry in the energy transfer to the rotating shaft occurs mainly about the regions with impulsive acceleration (see Fig. 2). As a consequence,

$$Q'_S = \int_0^{2\pi} \frac{\partial Q'_S}{\partial \phi} d\phi \ > \ 0 \,, \quad (30)$$

meaning that, after each complete turn, a net mechanical energy increase equal to Q'_S is brought to the rotor shaft.

V. Numerical example

The primary parameter for quantification of the analysis in the previous sections is B'_S, the oscillating magnitude of the magnetic flux aroused by mechanical vibrations.

If a working setup is available for open research, it should be possible to measure the value of B'_S. Alternatively, if $\Delta\phi'_S$ is measured (the peak-to-peak magnitude of the angular vibration), the value of B'_S can be fetched by try-and-error iterations, following the procedure below. Based on the value of B'_S, all the other coefficients for the previous equations can be obtained.

The geometric dimensions from Table 1 are applied in the sequence, being similar to the ones in [1].

For instance, if it is desired to have a flux mill that delivers P =500W mechanical power out of the rotor shaft at 1000rpm, the necessary total mechanical energy per turn, say Q_Σ, at $\omega = \frac{2\pi}{60}1000$ [rad/s], should be

$$Q_\Sigma = P/\omega = 4.77\,[J]. \quad (31)$$

TABLE I: Parameters and geometrical dimensions

Parameter		Value	Description
B_{re}	[T]	1.42	remanent magnetization NFeB 52
R_D	[mm]	2.5	PM disk radius
h_D	[mm]	2.0	PM disk height
r_C	[mm]	40	rotor radius
h_C	[mm]	45	rotor height
n	[-]	4	number of rotor rings with PM's
η	[-]	16	number of PM's per ring
P	[W]	500	rotor mechanical output power
rpm	[turns/min]	1000	shaft rotation speed

Since there are 64 (= $n \cdot \eta$) magnets inlaid on the rotor, the required energy increment per turn per magnet will be

$$Q'_S = \frac{Q_\Sigma}{64} = 74.6\,[mJ]. \quad (32)$$

Regarding (28), it results for $\eta = 16$ that

$$\frac{Q'_S}{Q_0} \;=\; \frac{1}{Q_0}\int_0^{2\pi} \frac{\partial Q'_S}{\partial \phi} d\phi \;= 50.27\,, \quad (33)$$

$$\Rightarrow Q_0 \;=\; \frac{1}{50.27} Q'_S = 0.0015. \quad (34)$$

To proceed, an attempt value for B'_S is needed. Let's try B'_S = 80mT, which is a small quantity if, for instance, the remanent flux density of the magnets in Table 1 is taken as reference (B_{re} = 1.42T).

Continuing,

$$F_0 \;=\; 2\frac{\eta\mu_C B'_S}{r_C} \;= 2.90\,, \quad (35)$$

$$\lambda \;=\; \frac{1}{8}\frac{r_C}{(\eta\mu_C B'_S)^2} Q_0 \;= 0.0022\,, \quad (36)$$

and the vibrating angle ϕ'_S is calculated from (24):

$$\phi'_S = \lambda\, F_r(\phi)\,,\ 0 \le \phi \le 2\pi\,, \quad (37)$$

as shown in Fig. 5.

At last, inspecting Fig. 5, we get with (25) that

$$\Delta\phi'_S = 0.0195\pi = 3.5^o\,, \quad (38)$$

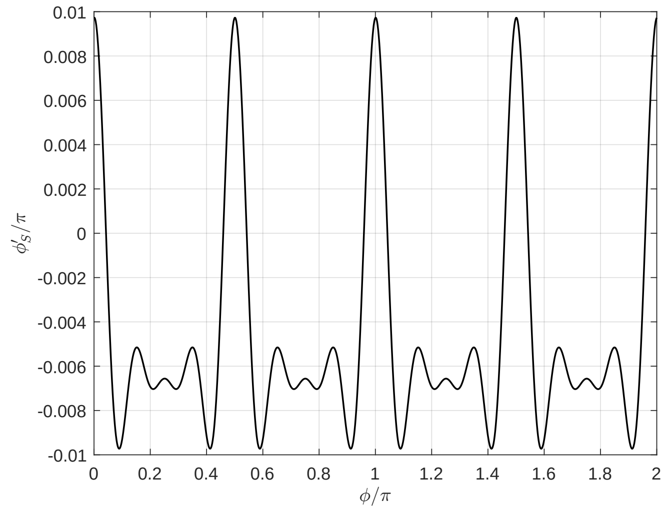

Fig. 5: Angular rotor disturbances. Eq.(24) with $\eta = 16$ and B'_S = 80mT.

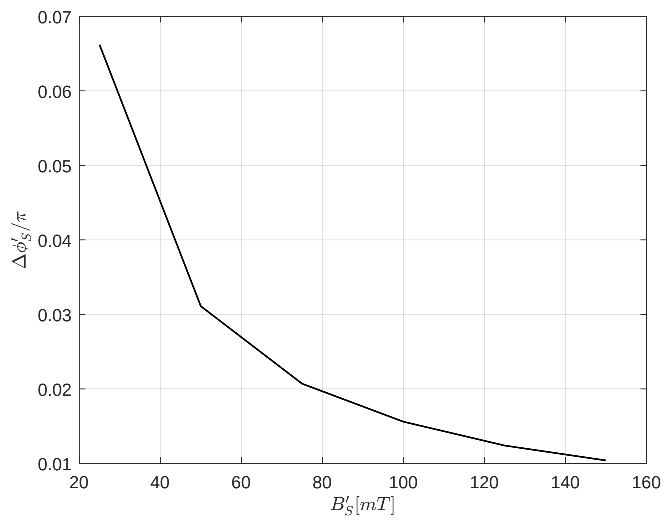

Fig. 6: Peak-to-peak angular vibration magnitude superposed on the rotor shaft , as function of oscillations in the magnetic flux magnitude. Eq.(25) with η =16 and P =500W at 1000rpm.

confirming that transfer of energy from the quantum vacuum could be realized based on narrow rotational vibrations in the construction of the flux mill.

Fig. 6 shows the sensitivity of $\Delta\phi'_S$ with respect of B'_S. The higher B'_S, the narrower the vibrations needed for generating the same power of 500W at 1000rpm.

VI. Conclusion

Applying the concepts of [4] to the situation of [1], it is hypothesized that mechanical vibrations and magnetic flux oscillations are cooperative in a magnetic-wind mill. The underlying premises are: (a) the magnitude of the external magnetic flux bears an oscillating *radial* component due to the low rigidity of the mechanical construction, and (b) the rotational motion has a vibrating *angular* component proportional to the *acceleration* of dynamic *radial* forces. In this way, a path is suggested for describing the transfer of energy from the quantum vacuum to the mill shaft.

A numerical example is detailed to check that the calculated peak-to-peak magnitude of the rotor's angular vibration has a small realistic value.

Appendix

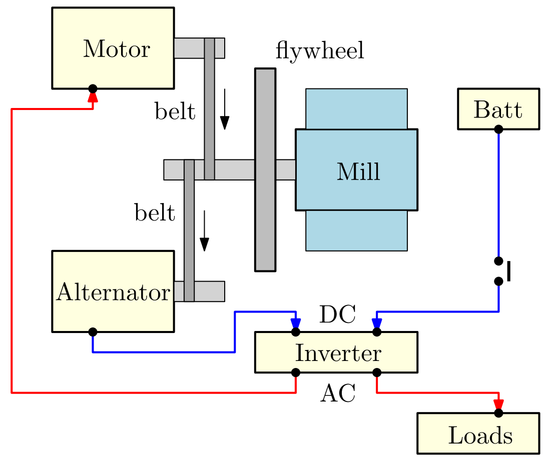

Fig. 7: General arrangement of the setup parts in [1].

Acknowledgements

The personal communications with Horst Eckardt were greatly appreciated.

References

[1] *Dicas do Leao, Self-sustained energy generator 4kW*, https://www.youtube.com/watch?v=IBV8Pg0RcII

[2] H. Eckardt, *Einstein-Cartan-Evans Unified Field Theory*, Feb 2022, ISBN-13: 978-3754949474

[3] *Dicas do Leao*,
(a) https://www.youtube.com/watch?v=pMD-GSjqqmc
(b) https://www.youtube.com/watch?v=HG32MoYXDbw

[4] J.L. Duarte, *Essay on magnetic-wind mills, Part II : Staying power from spacetime*, Feb 2023, https://aias.us/documents/otherPapers/..

[5] J.A. Barandes, *Can magnetic forces do work?*, Jul 2023, https://arxiv.org/abs/1911.08890

First appeared: November 9th, 2024[url]
This version: December 10th, 2024[url]

J.L. Duarte
magnetogenesis@proton.me